Schweizerische Eidgenossenschaft
Confédération suisse
Confederazione Svizzera
Confederaziun svizra

Federal Department of the Environment,
Transport, Energy and Communications DETEC

Swiss Federal Office of Energy
Energy Research and Cleantech

Final report from 14 November 2025

QUINPORTION

Measurement and Quantification of Inertia on Electrical Power Systems to Support Integration of Renewables

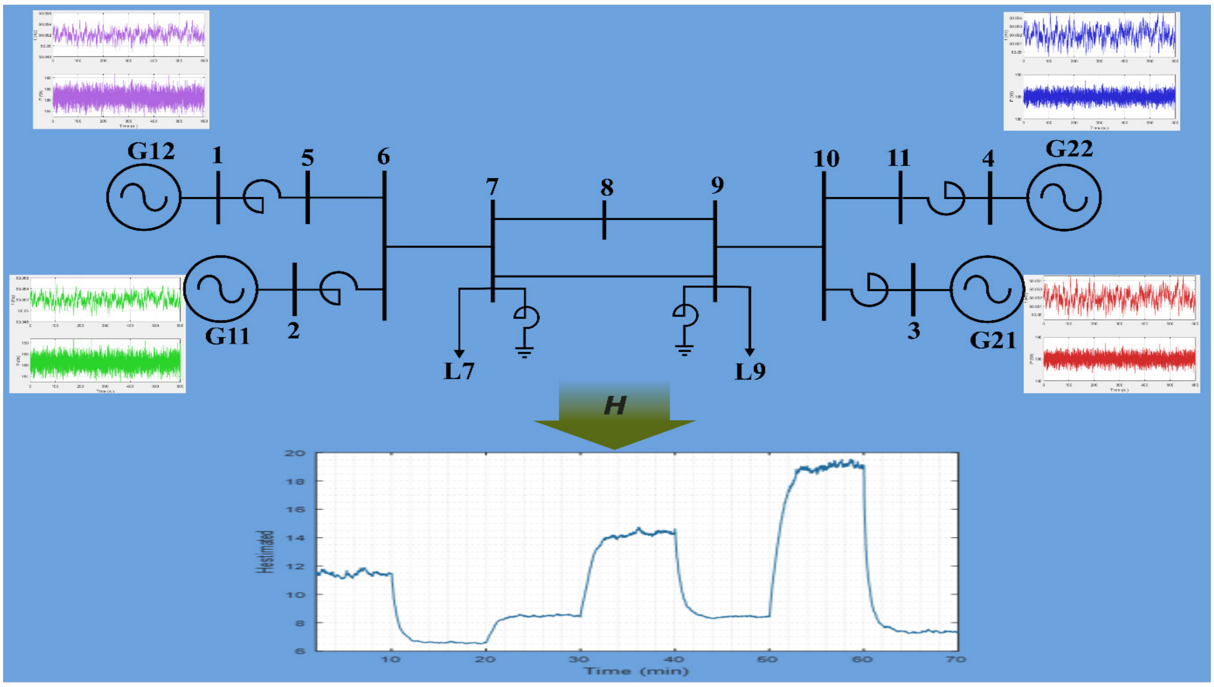

Publisher:
Swiss Federal Office of Energy SFOE
Energy Research and Cleantech
CH-3003 Berne
www.energy-research.ch

Subsidy recipients:
Zurich University of Applied Sciences (ZHAW)
Gertrudstrasse 15, CH-8401 Winterthur
www.zhaw.ch

Federal Institute of Metrology (METAS)
Lindenweg 50, CH-3003 Bern-Wabern
www.metas.ch

Authors:
Miguel Ramirez-Gonzalez, ZHAW, ramg@zhaw.ch
Guglielmo Frigo, METAS, Guglielmo.Frigo@metas.ch
Felix Rafael Segundo Sevilla, ZHAW, segu@zhaw.ch
Petr Korba, ZHAW, korb@zhaw.ch

SFOE project coordinator:
Dr. Michael Moser, michael.moser@bfe.admin.ch

SFOE contract number: SI/502415-01

Summary

Due to the increasing integration of power electronics-based renewable energy resources, the active quantification and monitoring of the available inertia to opportunely deploy support actions that can keep its value above critical levels is becoming more and more essential in modern power systems. Besides, since emerging operating scenarios are characterized by higher harmonic distortions and faster dynamics, the accurate tracking of the fundamental frequency and the ROCOF has become significantly challenging. Therefore, new measurement procedures and instruments are required to be developed and validated to equip system operators with more reliable measurements. The QUINPORTION project was centred on the development and full characterization of a new PMU prototype that not only meets the standard requirements but that is also designed to cope with the challenges of low-inertia networks. Besides, the other main focus of the project was the development, implementation, and assessment of suitable algorithms for the dynamic quantification of physical and virtual inertia in power systems.

According to this, an enhanced PMU was developed using the industrial controller NI cRIO-9054 and the Taylor-Fourier Multi-Frequency model for the estimation of phasor, frequency, and ROCOF. Among different examinations, the fidelity of the PMU measurements was evaluated within sophisticated Hardware-in- the-Loop testbeds. In this regard, the device was compared against a Schweitzer Engineering Laboratories SEL-421 protection, automation, and control system (which has an integrated PMU functionality conforming to the IEEE C37.118 standard). Based on different validation metrics, it was confirmed that the entire measurement chain (from the physical signals to the final processed metrics) operates with sufficient accuracy and low latency to be effective for real-time stability monitoring. Furthermore, by subjecting the PMU to realistic and severe grid dynamics in a controlled environment, it was verified that the physical hardware can deliver data of sufficient quality and timeliness. Obtained results in this sense represent a critical step in the technology readiness level, effectively de-risking the proposed solution and paving the way for pilot implementations with TSO partners.

Likewise, based on the results related to the estimation of inertia, performed off-line and real-time simulations demonstrated the effectiveness and accuracy of selected, recursive system identification approaches to approximate inertia in power systems. By using ambient frequency and active power measurements along with parametric model structures such as ARMAX, ARX, and OE, the capability of these forms for inertia extraction in a continuous and dynamic way was verified in a real-time simulation platform. The numerical accuracy, computational efficiency, and robustness of these alternatives is demonstrated by estimating the inertia constant of synchronous generators as well as the virtual contributions from an inverter-based resource with Virtual Synchronous Machine control. By this means, valuable insights into the practical aspects and potential of the chosen methods for actual, real-world power system applications, have been achieved.

Zusammenfassung

Aufgrund der zunehmenden Integration leistungselektronikbasierter erneuerbarer Energiequellen wird die aktive Quantifizierung und Überwachung der verfügbaren Trägheit in modernen Stromnetzen immer wichtiger. Da neue Betriebsszenarien durch höhere Oberwellenverzerrungen und schnellere Dynamik gekennzeichnet sind, stellt die präzise Erfassung der Grundfrequenz und des ROCOF eine erhebliche Herausforderung dar. Daher müssen neue Messmethoden und -instrumente entwickelt und validiert werden, um Netzbetreibern zuverlässigere Messwerte zu liefern. Das Projekt QUINPORTION konzentrierte sich auf die Entwicklung und umfassende Charakterisierung eines neuartigen PMU-Prototyps, der nicht nur die Standardanforderungen erfüllt, sondern auch auf die Herausforderungen von Netzen mit geringer Trägheit zugeschnitten ist. Ein weiterer Schwerpunkt des Projekts lag auf der Entwicklung, Implementierung und Evaluierung geeigneter Algorithmen zur dynamischen Quantifizierung der physikalischen und virtuellen Trägheit in Stromnetzen.

Demnach wurde ein verbessertes PMU unter Verwendung des Industriecontrollers NI cRIO-9054 und des Taylor-Fourier-Mehrfrequenzmodells zur Schätzung von Phasor, Frequenz und ROCOF entwickelt. Die Genauigkeit der PMU-Messungen wurde in Hardware-in-the-Loop-Testumgebungen evaluiert. Hierbei wurde das Gerät mit einem Schutz-, Automatisierungs- und Steuerungssystem SEL-421 von Schweitzer Engineering Laboratories verglichen, das über eine integrierte PMU-Funktionalität gemäss IEEE C37.118 verfügt. Anhand verschiedener Validierungsmetriken wurde bestätigt, dass die gesamte Messkette (von den physikalischen Signalen bis zu den verarbeiteten Metriken) mit ausreichender Genauigkeit und geringer Latenz arbeitet, um für die Echtzeit-Stabilitätsüberwachung effektiv zu sein. Darüber hinaus wurde durch die Anwendung realistischer Netzdynamiken in einer kontrollierten Umgebung verifiziert, dass die Hardware Daten von ausreichender Qualität und Aktualität liefert. Die erzielten Ergebnisse stellen in diesem Sinne einen entscheidenden Schritt im Hinblick auf den technologischen Reifegrad dar, indem sie das Risiko der vorgeschlagenen Lösung effektiv minimieren und den Weg für Pilotimplementierungen mit TSO-Partnern ebnen.

Die Ergebnisse der Trägheitsschätzung, die in Offline- und Echtzeitsimulationen erzielt wurden, demonstrierten die Effektivität und Genauigkeit ausgewählter, rekursiver Systemidentifikationsverfahren zur Trägheitsapproximation in Stromnetzen. Mithilfe von Umgebungsfrequenz- und Wirkleistungsmessungen sowie parametrischen Modellstrukturen wie ARMAX, ARX und OE wurde die Fähigkeit dieser Verfahren zur kontinuierlichen und dynamischen Trägheitsbestimmung in einer Echtzeitsimulationsplattform verifiziert. Die numerische Genauigkeit, Recheneffizienz und Robustheit dieser Alternativen wurden durch die Schätzung der Trägheitskonstante von Synchrongeneratoren sowie der virtuellen Beiträge einer wechselrichterbasierten Ressource mit Virtual Synchronous Machine-Regelung demonstriert. Dadurch wurden wertvolle Erkenntnisse über die praktischen Aspekte und das Potenzial der gewählten Methoden für reale Anwendungen in Stromnetzen gewonnen.

Résumé

Avec l'intégration croissante des énergies renouvelables basées sur l'électronique de puissance, la quantification et la surveillance actives de l'inertie disponible deviennent essentielles dans les réseaux électriques modernes. De plus, face aux nouveaux scénarios d'exploitation caractérisés par des distorsions harmoniques plus élevées et une dynamique plus rapide, la surveillance précise de la fréquence fondamentale et du ROCOF représente un défi majeur. Par conséquent, de nouvelles procédures et de nouveaux instruments de mesure doivent être développés et validés afin de fournir aux gestionnaires de réseau des mesures plus fiables. Le projet QUINPORTION était axé sur le développement et la caractérisation complète d'un nouveau prototype de PMU répondant aux exigences normatives et conçu pour relever les défis posés par les réseaux à faible inertie. L'autre axe majeur du projet a été le développement, la mise en œuvre et l'évaluation d'algorithmes adaptés à la quantification dynamique de l'inertie physique et virtuelle dans les réseaux électriques.

Conformément à ces travaux, une PMU améliorée a été développée à l'aide du contrôleur industriel NI cRIO-9054 et du modèle multifréquence de Taylor-Fourier pour l'estimation des phaseurs, de la fréquence et du ROCOF. Parmi les différents tests réalisés, la fidélité des mesures de la PMU a été évaluée au sein de bancs d'essai sophistiqués de type « Hardware-in-the-Loop ». À cet égard, le dispositif a été comparé à un système de protection, d'automatisation et de contrôle Schweitzer Engineering Laboratories SEL-421 (qui intègre une PMU conforme à la norme IEEE C37.118). Différentes métriques de validation ont confirmé que l'ensemble de la chaîne de mesure (des signaux physiques aux métriques finales traitées) fonctionne avec une précision suffisante et une faible latence pour une surveillance efficace de la stabilité en temps réel. De plus, en soumettant la PMU à des dynamiques de réseau réalistes et sévères dans un environnement contrôlé, il a été vérifié que le matériel physique peut fournir des données de qualité et de réactivité suffisantes. Les résultats obtenus à cet égard représentent une étape cruciale dans le niveau de maturité technologique, réduisant efficacement les risques liés à la solution proposée et ouvrant la voie à des mises en œuvre pilotes avec les partenaires TSO.

De même, à partir des résultats concernant l'estimation de l'inertie, des simulations hors ligne et en temps réel ont démontré l'efficacité et la précision des approches d'identification de systèmes récursifs pour l'approximation de l'inertie dans les réseaux électriques. L'utilisation de mesures de fréquence ambiante et de puissance active, ainsi que de modèles paramétriques tels que ARMAX, ARX et OE, a permis de vérifier, sur une plateforme de simulation en temps réel, la capacité de ces modèles à extraire l'inertie de manière continue et dynamique. La précision numérique, l'efficacité de calcul et la robustesse de ces alternatives sont démontrées par l'estimation de la constante d'inertie des générateurs synchrones et des contributions virtuelles d'une ressource pilotée par onduleur avec commande de machine synchrone virtuelle. Ainsi, des informations précieuses ont été obtenues concernant les aspects pratiques et le potentiel des méthodes choisies pour des applications réelles dans les réseaux électriques.

Main findings («Take-Home Messages»)

- Since local inertia estimation is greatly affected by disturbances and on-going dynamics, robust and accurate measurements of frequency, ROCOF, and power are required, which calls for enhanced and more robust PMUs.
- Quantities like ROCOF are very difficult to be estimated in real-time during disturbances. However, the aggregation of measurements according to a given criteria allows for producing good estimates of ROCOF in a limited and consistent geographical area.
- By using ambient measurements from PMUs, recursive polynomial model estimators can be used to continuously extract in real-time implicit inertia values, including time varying values of virtual inertia contributions from CIG with VSM control.
- The validation of algorithms in real-time simulation environments and Hardware-in-the-Loop setups provides the ability for practical performance and robustness assessment under realistic operational constraints, as well as the detection of critical issues for real-world deployment.

Contents

List of figures

List of tables

List of abbreviations

ARX	Auto-Regressive with Exogenous Input
ARMAX	Auto-Regressive Moving-Average with Exogenous Input
BESS	Battery Energy Storage System
CIG	Converter-Interfaced Generator
CNN	Convolutional Neural Network
EKF	Extended Kalman Filter
EMT	Electromagnetic Transient
EWTFM	Enhanced Windowed Taylor-Fourier Multi-Frequency Model
FE	Frequency Error
FIFO	First-In First-Out
FPGA	Field Programmable Gate Array
GTAI	Giga-Transceiver Analogue Input
HIL	Hardware-in-the-Loop
LPIT	Low Power instrument Transformer
ML	Machine Learning
MLP	Multilayer Perceptron
NN	Neural Network
NA	Not applicable
NPL	National Physical Laboratory
OE	Output Error
PMU	Phasor Measurement Unit
PTP	Precision Time Protocol
RES	Renewable Energy Source
RFE	ROCOF Error
ROCOF	Rate of Change of Frequency
SFOE	Swiss Federal Office of Energy
SG	Synchronous Generator
SINAD	Signal-to-Noise-and-Distortion
SVM	Support Vector Machine
TSO	Transmission System Operator
TVE	Total Vector Error
TFM	Taylor Fourier Multi-Frequency Model
UFLS	Under-Frequency Load Shedding
VSM	Virtual Synchronous Machine
ZHAW	Zurich University of Applied Sciences

1 Introduction

1.1 Context and motivation

Due to carbon footprint issues, modern power systems have been permeated by a considerable amount of inverter-based renewable energy sources that do not provide any rotational inertia [1], [2]. As a consequence, the grid is becoming more and more vulnerable to rapid frequency excursions that lead to high rates of change of frequency (ROCOFs) and deep frequency nadirs [3], [4]. Furthermore, converter's power electronic circuitry, with switches at high frequency, introduces harmonic and inter-harmonic pollution into the network [5]. In such a challenging scenario, a reliable measurement infrastructure that enables the application of wide-area monitoring and control systems for improved situational awareness turns out to be critical. In this regard, Phasor Measurement Units (PMUs) have become an essential actor in contemporary power systems because they can provide high-speed, synchronized, real-time measurements over wide geographical areas, which is essential to effectively monitor the increasingly complex and dynamic grid. Moreover, by using PMU measurements, it can be possible to estimate the instantaneous inertia levels of the network and apply them to deploy additional inertia resources [6].

Because of the increasing level of harmonic distortion and faster dynamics in current and foreseen operating scenarios [7], the traditional and pure sinusoidal model for the power signal is becoming insufficient for effective analysis and design. Therefore, new approaches and technologies are necessary to address the issues related to the accuracy, reliability, and quality of the measurements [8]. According to this, PMUs must be fast enough to capture both the instantaneous frequency and its rate of change during system dynamics, and accurate/robust enough to ignore noise and interference. Scientific literature, as well as the instrument market, propose a wide variety of solutions that are compliant with the international standard IEC/IEEE Std 60255-118-1:2018 [9], where the requirements for synchronized phasor measurement systems in electrical transmission networks are defined. However, while the standard covers dynamic performance, the behavior and accuracy requirements for synchrophasor, frequency, and ROCOF measurements may be inadequate for certain transients. A series of recent contingencies in South Australia and Europe are proof of the current need for more sophisticated instruments, which can attend the limitations of the standard in this sense.

Based on the considerations above, the monitoring and control of inertia is a crucial demand to maintain a reliable, stable, and secure electricity supply in the evolving grid. However, despite different inertia estimation methos found in the literature, most of them are based on offline data processing and analysis or fail to account for virtual inertia from inverter-based resources. Basically, they underestimate critical timing and practical system integration issues, and provide very limited or no insights at all into the suitability of the methodology for the continuous quantification of inertia under ambient conditions. On the other side, as fast transient conditions and off-nominal frequencies are more prevalent in modern, low-inertia systems, enhanced or specialized PMU designs and algorithms are needed to address specific performance gaps and emerging requirements. According to this, a new PMU prototype was developed, characterized, and validated in this project with the intention to equip system operators with more reliable measurements. On the other hand, different methods to track and quantify physical and virtual inertia in power systems were first studied offline and then implemented in real time to assess their viability, speed, robustness, and integration capability for practical deployment.

1.2 Project objectives

The project represents a first feasibility assessment of PMU-based control of low-inertia power systems, as it aims to evaluate how the PMU measurement uncertainty propagates in the different stages of the monitoring and control applications. Such a result promises to be extremely helpful and profitable from both the system operator and instrument manufacturer point of view, as it will highlight still open issues as well as space for enhancement. Moreover, the development of new PMU-based solutions will facilitate the international cooperation within the CIGRE/IEEE joint working group C4/C2.62, the IEC TC 8JWG 12, and the IEEE Working Group on Application of Big Data Analytic for Transmission Systems.

The new PMU prototype was intended to be characterized by high accuracy in dynamic conditions (e.g. frequency errors in the order of 100 mHz during sinusoidal or quadratic phase modulations) as well as reduced latency (i.e. in the order of few tens ms). In this way, PMU frequency measurements can allow for a more precise and prompter identification of network inertia modifications and thus a more effective counteraction. By means of hardware-in-the-loop simulations, the prototype was not only evaluated in standard test conditions but also in realistic operating conditions. Indeed, a crucial point for the development of this technology was the assessment of its reliability when deployed on the field. A clear understanding of which phenomena can be properly captured, and which produce inaccurate estimates, allowed the definition of a confidence interval of PMU estimates for different applications (inertia monitoring, protection, etc.). Indeed, the expected outcome was the development and full characterization of a new PMU prototype that not only meets the standard requirements but that is also designed to cope with the challenges of low-inertia networks.

The research work carried out in this project was conceived according to the following main objectives:

- Development of a novel PMU prototype, more resilient with respect to harmonic distortion and capable to cope with amplitude and phase fluctuations, for inertia estimation applications.
- Definition and development of inertia measurement methods that rely on PMU measurements and account for their inherent uncertainty in the different stages of monitoring and control.
- Demonstration of the feasibility and reliability of the proposed approaches by means of laboratory testing and Hardware-in-the-Loop realization.

2 Approach, method, results and discussion

The considered approaches and methods, and obtained results, are presented according to the main contributions achieved during the three-year duration of the project. In this context, the development and characterization of the enhanced PMU, including the estimator for the PMU algorithm, the assessment of performance and reliability of the entire measurement and analysis chain, as well as the validation against commercial hardware, are described on one side. On the other side, the part related to the algorithms for the dynamic monitoring and quantification of inertia in power systems is described according to the literature review of existing algorithms, the offline implementation and evaluation of some of them, and the online and real-time assessment of structures such as ARX, ARMAX, and OE models for continuous inertia estimation.

2.1 PMU prototype development and characterization

The development of novel grid monitoring and stability assessment tools based on PMU data is a cornerstone of modernizing power system operations. While offline simulations and theoretical analyses are essential for initial development, they cannot fully capture the complexities and imperfections of real-world implementation. These include hardware processing delays, communication latency, data packet loss, measurement noise, and the specific characteristics of physical measurement devices. To bridge this critical gap between simulation and real-world deployment, a rigorous Hardware-in-the-Loop (HIL) validation was conducted.

2.1.1 Enhanced PMU device

For this analysis, an enhanced PMU device has been developed and characterized. In this context, Fig. 1 presents the conceptual scheme of the PMU device.

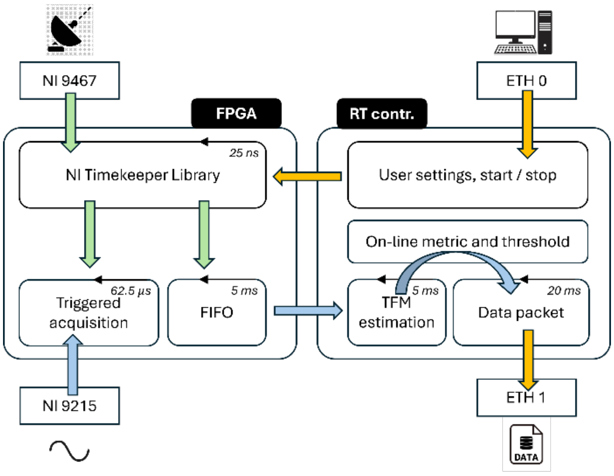

Fig. 1 Conceptual block scheme of the PMU developed for HIL testing.

The QUINPORTION PMU (briefly, H-PMU) relies on a NI cRIO-9054 (National Instruments, Austin, US-TX) equipped with a Linux Real-Time (RT) operating system and a re-configurable Field Programmable Gate Array (FPGA) board. The former is a 1.33-GHz dual-core Intel Atom E3805 processor. The FPGA board is a Xilinx Artix-7 100T, with 240 DSP slices and over 63000 LUTs. The H-PMU is equipped with an Ethernet board with two channels, ETH0 and ETH1, for the communication with an external PC and the transmission of data packets, respectively. The NI cRIO-9054 also embeds two external modules: a NI 9467 synchronization module and a NI 9215 voltage input module. The H-PMU code has been developed in LabVIEW 2024.

Via ETH0, the user sets the threshold limits for the detection of anomalous conditions and starts the measurement process. This operation initiates the synchronization process: the NI 9467 module serves as a GPS receiver, while the NI Timekeeper library allows one to define an internal timebase and retrieve a timestamp, both locked to UTC. This process runs in a separate loop, whose resolution is limited only by the FPGA internal clock (25 ns). Once completed, the variable "FPGA Timekeeper locked" is set to true, and the acquisition process is initiated. In this case, the NI 9215 controls three input channels: a0 is intended to detect external trigger signals (e.g., TTL signals), while a1 and a2 acquire two input signals like the output of a low power instrument transformer (LPIT) for voltage or current, respectively. All channels are sampled synchronously at 16 kHz, with a fixed input range of ±7 V and a resolution of 16 bits. This process runs in a timed loop (with a period of 62.5 μs) to lock the sampling rate to the Timekeeper timebase.

The acquired data are stored in a dedicated First-In First-Out (FIFO) structure. With a fixed period of 5 ms, the FIFO is stored with a cluster containing 80 samples acquired on ai1 and ai2, and an updated time-stamp as given by the Timekeeper library. On the RT controller side, the FIFO is read, and the data are unbundled. For each channel, the samples are inserted in a dedicated queue with a fixed length of 1200 samples, which corresponds to 75 ms. At each reporting interval (i.e., every 20 ms), the samples in the queue are processed by the estimation algorithm in [E]. The estimated phasor, frequency, and ROCOF allow for recovering the estimated input signal. The nRMSE metric quantifies the discrepancy between the acquired and recovered input signals. In this device, the same quantity is normalized by the magnitude of the estimated phasor and expressed in dB. In this way, the metric can be considered as an estimate of the Signal-to-Noise-and-Distortion (SINAD) index, which accounts for all the energy not mapped by the PMU representation of the fundamental component. In normal operations, the estimated SINAD should account only for uncorrelated noise (e.g. quantization noise), whereas it should degrade significantly in the case of spurious contributions or inaccurate measurement results.

Once completed the estimation process, the measurement results are encapsulated in a data packet as per the PMU Prot via the Electrical Power Toolkit library. More precisely, the estimated phasor, frequency, and ROCOF are stored in the fields PHASOR, FREQ, and DFREQ, respectively. The estimated SINAD, instead, is stored in an ANALOG field. Moreover, the estimated quantities are compared against a set of user-defined thresholds. Fig. 2 presents the rules for the detection of anomalous events. Once an event is detected, the last two bits of the STAT_FLAG word are set to 01, reserved for internal PMU errors. Data should be used with caution. Based on the type of event, more information is provided. If the phasor magnitude or the frequency exceeds their valid variation range, the Data Error bits in their respective attribute fields (i.e., DAPHASOR and DAFREQ) are activated. If the SINAD is too low, the Step Detected bit in the ROCOF attribute field (i.e., DADFREQ) is activated.

Parameter	Valid Range	Field
ph. mag.	[0.2 1.2] pu	DAPHASOR (Data Error)
frequency	[47.5 52.5] Hz	DAFREQ (Data Error)
SINAD	[70 96] dB	DADFREQ (Step Detected)

Fig. 2 Event detection rules as per IEEE C37.118.2 packet format.

The ranges allowed for each parameter are user defined, but are typically inspired by the traditional power systems' operation or by the H-PMU hardware configuration. Indeed, the magnitude range is the one considered in LPIT type testing, or the frequency range corresponds to most breaker withstand capability. Regarding the SINAD, 96 dB corresponds to the ideal quantization noise of a 16-bit digitizer, while the lower limit is set to 70 dB (assuming a normal operation at 80 dB).

2.1.2 PMU Algorithm

The estimation of phasor, frequency, and ROCOF relies on a Taylor-Fourier Multifrequency (TFM) estimator, optimized for a suitable trade-off between complexity and accuracy. This estimator, originally introduced in [D], allows for compensating both short- and long-range spectral leakage by means of a series of flat differentiator filters.

In particular, we consider a TFM implementation where the signal spectral support (i.e., the set of most significant component frequencies) is fixed: it includes the nominal system rate (50 Hz) and the harmonic components up to the fifth order (i.e., 100, 150, 200, and 250 Hz). The expansion order for the fundamental component is set to 3, while for odd and even harmonics it is limited to 2 and 1, respectively. To minimize spectral leakage from interfering tones that are not included in the spectral support, the input signal is previously multiplied by a weighing function, namely a Chebyshev window with 40 dB sidelobe attenuation.

Fig. 3 presents the performance of the H-PMU in all the tests of the IEC 60255-118-1:2018 with respect to P-class (protection) requirements. The reported errors refer to the standard metric Total Vector Error (TVE), Frequency Error (FE), and ROCOF Error (RFE), as well as an error on the estimation of the nRMSE in SINAD format, also known as SINAD Error (SINADE). All metrics prove to be way within the standard limits for TVE, FE, and RFE, according to the Std columns in Fig. 3.

Test	TVE (%)	Std (%)	FE (mHz)	Std (mHz)	RFE (Hz/s)	Std (Hz/s)	SINADE (dB)
nominal	0.0005	1	0.042	5	0.002	0.4	0.28
sig. frequency ($f_0 \pm 2$ Hz)	0.0130	1	0.289	5	0.017	0.4	0.83
harm. dist. (THD = 1%, f_0)	0.0193	1	0.531	5	0.216	0.4	0.51
harm. dist. (THD = 1%, $f_0 \pm 2$ Hz)	0.0303	1	3.630	5	0.327	0.4	0.91
ampl. mod. ($f_m = 2$ Hz)	0.0110	3	0.201	60	0.020	2.3	0.44
phase mod. ($f_m = 2$ Hz)	0.0152	3	0.206	60	0.045	2.3	1.18
freq. ramp ($\Delta f = \pm 2$ Hz/s)	0.0132	1	0.092	10	0.178	0.4	1.28

Fig. 3 Worst-case errors of the H-PMU algorithm as per IEC 60255-118-1:2018.

2.1.3 HIL tests

This section details the comprehensive validation of the proposed PMU-based stability and event detection metrics. The primary objective of this HIL testing phase was to de-risk the technology by assessing the performance and reliability of the entire measurement and analysis chain in a realistic, yet controlled, environment. By interfacing a commercial-grade PMU with a real-time power system simulator, we were able to evaluate the fidelity of the physical device's measurements against a known "ground truth" from the simulation. This process is crucial for building confidence among Transmission System Operators (TSOs) and proving the practical viability of these advanced monitoring techniques for enhancing grid visibility and security. The validation was performed at the University of Strathclyde, leveraging its state-of-the-art real-time simulation facilities.

A sophisticated HIL testbed was architected to emulate the end-to-end data flow from a transmission network substation to a control centre application. The setup comprised three main integrated components: a real-time digital simulator, the physical hardware under test, and a data acquisition and processing system.

The core of the testbed is the RTDS Simulator, a powerful platform capable of simulating complex power system electromagnetic transients in real-time. For this study, the RTDS was programmed with a detailed model of a microgrid as shown in Fig. 4.

The microgrid is modelled based on a European medium voltage test feeder described in the Cigré Technical Brochure 575. The system is rated at 20 kV with a nominal frequency of 50 Hz. The microgrid consists of nine nodes, with a total load of 4.55 MVA. In addition, there are three distributed energy resources: a synchronous generator of 5 MVA (slack machine), a photovoltaic (PV) generator of 1 MW, and a battery energy storage system (BESS) of 1 MVA.

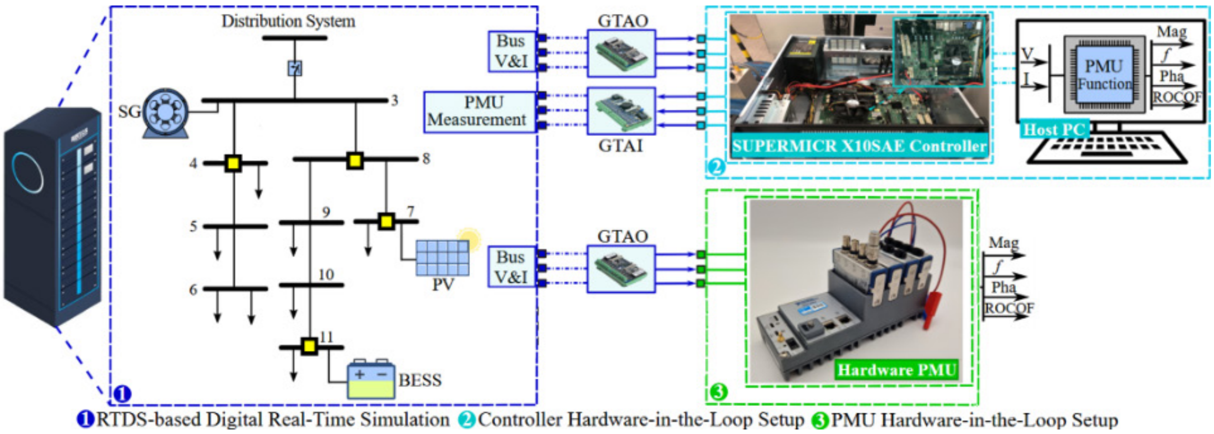

Fig. 4 Hardware in the Loop setup as used at Strathclyde University.

The synchronous generator inertia constant is varied within [0.5,1.0,1.5] s. The yellow squares denote the buses monitored by the PMU prototypes. In each node of interest, phase-locked loop and RMS measurement blocks are employed to retrieve the reference values for voltage and current signals.

For each simulated scenario, the voltage and current signals of interest are transferred in parallel to both the S-PMU and the H-PMU. The hardware and software implementations of the PMU serve a set of complimentary requirements. The hardware H-PMU is meant to prove the feasibility of such sophisticated estimation algorithms in market available industrial controllers. The software S-PMU is used as validation of the hardware one, since it relies on a much higher computational power, but is also used to populate more sophisticated network simulations with many PMUs (unfeasible with hardware devices because of the increased costs of realization and cabling). The S-PMU runs in real-time on a Supermicro X10SAE controller that connects with a host PC where the S-PMU is implemented and compiled. The Supermicro X10SAE controller guarantees a continuous link between the RTDS and the

S-PMU host PC. On one side, it acquires the RTDS signals from a Giga-Transceiver Analogue Output (GTAO) card in RTDS, and transfer them to the host PC. On the other side, it converts the measurement results into analog signals, which are acquired by the RTDS via a Giga-Transceiver Analogue Input (GTAI) card. In a similar way, the same RTDS signals are also supplied to the H-PMU by another GTAO card.

In this context, we reproduce a scenario where a fault occurs at Bus 09 at t = 4 s, producing a system split. In the lower portion of the system, the BESS is unable to sustain the operation, thereby leading to a blackout. On the other side, in the upper portion of the grid, the microgrid experiences remarkable oscillations but is capable of reaching a new equilibrium point.

Now, Fig. 5 proves the significant correlation between SINAD and PMU estimation accuracy. Fig. 5 (a) presents the PMU estimates of frequency in all considered buses. The measurement at Bus 11 is terminated in correspondence with the fault occurrence, as the microgrid portion downstream with respect to the fault locations experiences a blackout. Fig. 5 (b) presents the FEs of PMUs with respect to the ground truth value provided by the RTDS model. Finally, Fig. 5 (c) presents the corresponding SINAD estimates. In the pre-fault time interval, FE and SINAD keep within the expected limits (i.e., lower than 5 mHz and higher than 70 dB). After the fault occurrence, the SINAD decrease corresponds exactly to the FE degradation. By looking at the SINAD estimates, it is possible to infer the discrepancy between the PMU signal model and the actual acquired signal, thus predicting a plausible error range on its estimates. Once the SINAD has come back within its limit, the FE also proves to be compliant with the P-class requirements. This consideration applies to all PMUs, regardless of their proximity to the fault locations.

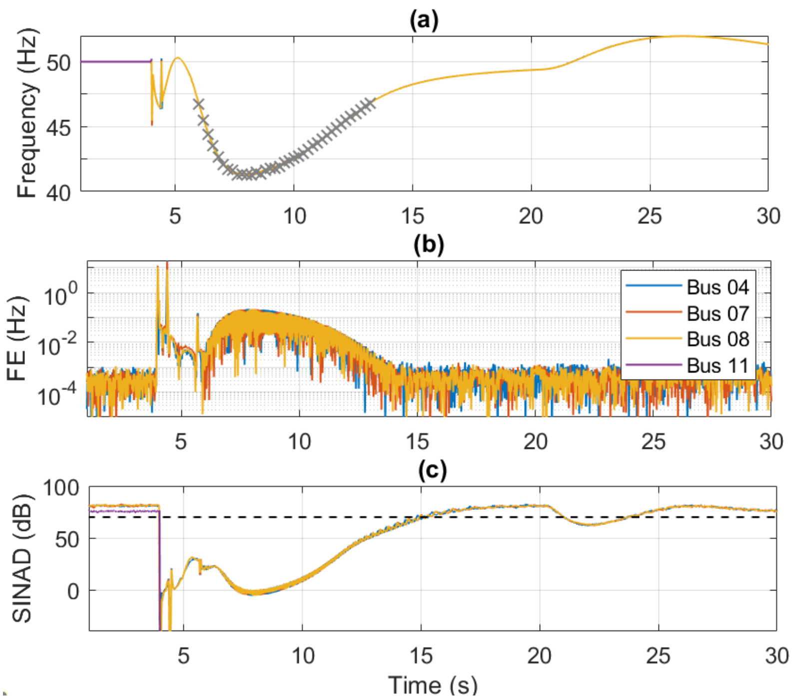

Fig. 5 Frequency estimates (a), frequency errors (b), and corresponding SINAD estimates (c) in a HIL simulation of the microgrid in Fig. 4.

2.1.4 Validation against commercial hardware

The physical device under test was compared against a Schweitzer Engineering Laboratories SEL-421 protection, automation, and control system, which has an integrated PMU functionality conforming to the IEEE C37.118 standard. The amplified voltage and current signals from the RTDS, representing the conditions at a specific bus in the simulated network, were fed directly into the analogue inputs of the

SEL-421. This setup forces the physical device to operate as if it were installed in a real substation, measuring dynamic grid conditions.

Precise time synchronization is fundamental to PMU technology. A Meinberg LANTIME M300 GPS clock served as the master clock for the entire testbed. It provided a highly accurate time reference to both the RTDS Simulator (ensuring the simulation timeline was precisely controlled) and the SEL-421 PMU via the Precision Time Protocol (PTP). This ensured that the timestamps applied to the PMU measurements were perfectly aligned with the timing of events within the simulation, allowing for a direct and meaningful comparison. The SEL-421, acting as a PMU, streamed its synchrophasor data packets over an Ethernet network using the IEEE C37.118.2 protocol at a reporting rate of 50 frames per second.

The core of the validation involved a direct comparison between the "ground truth" values, calculated within the RTDS simulation, and the corresponding values measured and streamed by the physical SEL-421 PMU. According to this, Fig. 6 (a) illustrates the deviations in the voltage magnitude estimates of the S- and H-PMU (in blue and red respectively), as compared to the expected nominal value (dashed black line). As it can be observed, the two PMU measurement results show similar variation ranges. This is further confirmed by the histogram representation in Fig. 6 (b), where the magnitude deviations have a very similar distribution.

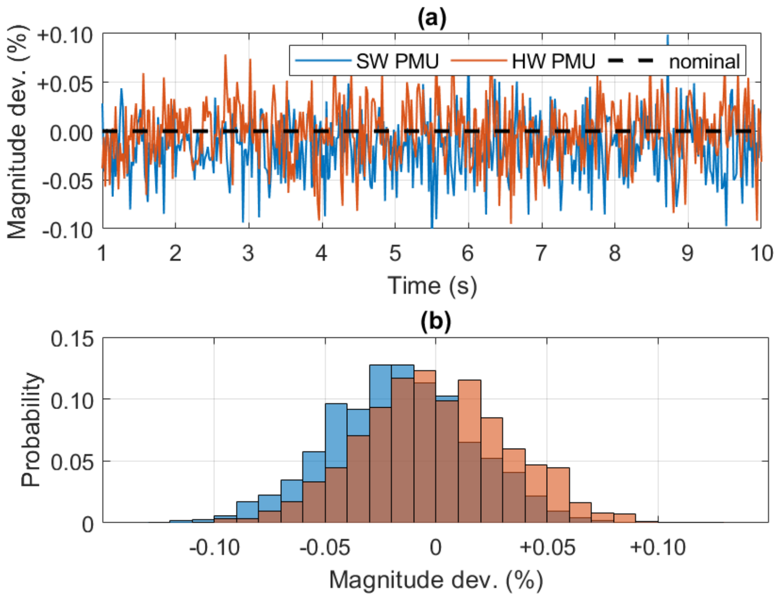

Fig. 6 Deviations in voltage estimates (a), and distribution of deviations (b).

The comparison for frequency and ROCOF was also excellent. The PMU's frequency measurement accurately tracked the simulated system frequency, capturing the post-fault frequency drop and subsequent recovery oscillations. Crucially, the ROCOF metric, which is highly sensitive to measurement noise and filtering, also showed a very strong correlation. The PMU-derived ROCOF closely matched the ground truth from the RTDS, albeit with a slight delay and smoothing effect attributable to the internal filtering and processing algorithms of the SEL-421. This result confirms that commercial PMUs are capable of providing reliable ROCOF data for frequency stability monitoring.

The voltage magnitude measurements from the PMU precisely captured the severe voltage dip during the fault and the subsequent recovery dynamics. This high-fidelity voltage measurement is essential for many stability applications. Furthermore, the apparent impedance trajectory, calculated from the PMU's voltage and current phasors, was compared against the theoretical impedance seen from Bus 5. The trajectories matched almost perfectly, demonstrating that the PMU provides the necessary data quality for advanced applications like out-of-step protection or voltage stability assessment, which rely on accurate impedance tracking.

The metrics related to active and reactive power fluctuations, designed to detect power swings and other dynamic instabilities, were also successfully validated. The values calculated from the PMU data stream closely followed the power dynamics observed in the RTDS simulation. This confirmed that the entire measurement chain—from the physical signals to the final processed metrics—operates with sufficient accuracy and low latency to be effective for real-time stability monitoring.

The Hardware-in-the-Loop validation campaign successfully demonstrated the real-world feasibility and reliability of the developed PMU-based monitoring metrics. By subjecting a commercial PMU to realistic and severe grid dynamics in a controlled environment, we confirmed that the physical hardware can deliver data of sufficient quality and timeliness. The close agreement between the PMU measurements and the RTDS ground truth across all tested metrics instils high confidence in their potential for deployment in operational environments. This work represents a critical step in the technology readiness level, effectively de-risking the proposed solution and paving the way for pilot implementations with TSO partners.

2.2 Measurement and quantification of inertia in power systems

The large-scale integration of renewable energy resources through converter-interfaced generators (CIGs) is imposing new challenges considering power system frequency dynamics and stability. Since a decline in overall system inertia is undergone as synchronous machines are gradually and correspondingly displaced, an unacceptable ROCOF and important frequency deviations may occur after a relatively significant imbalance between system generation and load, leading to potential and uncontrolled cascading failures, and eventually a system collapse [10].

Due to the relevance of an adequate inertia to counteract and control initial changes in grid frequency, grid operators are already facing inertia-related challenges to avoid electricity service interruptions under operating scenarios with significant shares of non-synchronous energy sources. Therefore, the active quantification and monitoring of the available inertia to opportunely deploy support actions that can keep its value above critical levels has become a key issue for grid stability [11]-[13].

In general, inertia is critical for maintaining the stability, reliability, and security of power systems. In this way, the more inertia the system has, the better the capability of the grid to resist dynamic changes [10]. Basically, the inertial response has to do with the immediate power system reaction to frequency deviations. It depends on the rotational energy stored in the rotors of the synchronous machines and affects the initial ROCOF following a sudden active power imbalance.

The basic equation that governs the rotor dynamics of synchronous generators (SGs) is called the swing equation, which can be expressed in p.u. according to:

$$2H\frac{d\Delta\omega}{dt} = \Delta P_{\mathrm{m}} - \Delta P_{\mathrm{e}} - D\Delta\omega \tag{1}$$

where $\Delta\omega$ is the speed deviation, H is the inertia constant, D is a damping factor, and ΔP_{m} and ΔP_{e} denote correspondingly the change in mechanical and electrical power. Based on (1), different strategies can be followed to approximate the inertia constant. For example, by neglecting the damping term and assuming that immediately after a large disturbance $\Delta P_{\mathrm{m}} \approx 0$, a simplified version can be achieved:

$$2H\frac{d\Delta\omega}{dt} = -\Delta P_{\mathrm{e}} \tag{2}$$

Now, considering that the speed and frequency deviations are equivalent in p.u., then an approximation in terms of Δf can be derived, as follows:

$$\frac{d\Delta f}{dt} = \frac{-\Delta P_{\mathrm{e}}}{2H} \tag{3}$$

It can be inferred from (3) that, after a sudden generator disconnection or load tripping, the initial ROCOF in a power system will be influenced significantly by a large difference between the generated and consumed electrical power. In this case, the ROCOF can be considerably high if the aforementioned incidents take place in particular regions with a relatively small inertia constant, where the equivalent rotating mass is given by:

$$H = \frac{\sum_i^G H_i \cdot S_{ni}}{S_B} \quad (4)$$

with G being the number of SGs, and H_i and S_{ni} representing respectively the inertia constant and rated power (MVA) of a given generator i. Regarding (3), the equation can be solved for H to obtain the following:

$$H = -\frac{1}{2}\frac{\Delta P_e}{\frac{df}{dt}} \quad (5)$$

where ΔP_e and $\frac{df}{dt}$ can be directly determined according to information from the given disturbance and approximated ROCOF. On the other side, by following some similar previous assumptions but working with the Laplace Transform of (1), a relationship between change in frequency and change in electrical power can be found:

$$\frac{\Delta f(s)}{\Delta P_e(s)} = \frac{-\frac{1}{2H}}{s+\frac{D}{2H}} \quad (6)$$

where H can be determined from an equivalent discrete-time model using system identification techniques.

2.2.1 Algorithms for inertia approximation based on PMU measurements

According to [14], the alternatives for inertia estimation can be divided in general as model-based approaches and measurement-based approaches. Since pure model-based methods completely rely on a dynamic model of SGs and equivalent system behavior, the mathematical model´s accuracy will highly influence the estimation to achieve. Furthermore, these methods may fail to estimate virtual inertia from CIGs if the associated dynamics are not included somehow in the considered representation. Therefore, measurement-based methodologies are preferred since they rely on actual measured data instead of on pre-existing system information and exact mathematical modelling. Measurement-based alternatives can be further classified according to the operating condition (disturbance versus ambient) and the underlaying technique.

In general, several strategies for inertia estimation using PMU measurements can be found in the literature. For example, ambient measurements from PMU and a model identification process are proposed in [15] for this purpose, where changes in active power and resulting frequency deviations are used to identify ARMAX models of various orders, and inertias values are extracted from the impulse response of first order transfer functions derived from preselected ARMAX structures. Since the estimation results in that case are highly associated with a correct order of the identified models, a related but modified approach is proposed in [16], where the maximum ROCOF computed from the step response of identified transfer functions is used to quantify the inertia constant based on (5), neglecting the initial excursions up to a given time. According to that, better consistency in terms of accuracy of results was observed for the different model orders assumed in the study. In [17], an alternative based on the extended Kalman Filter (EKF) and a window-based method was adopted to determine the inertia of a synchronous generator in real time. The proposed EKF technique relies on a given mathematical model to describe the dynamic behaviour of the corresponding generator after an unbalancing event. On the other hand, by considering a dynamic network equivalent around generic buses with PMUs and using perturbations caused by generator outages and load disconnections, equivalent machines are obtained at monitored buses in [18]. Then, by formulating the swing equations associated with these equivalents, computing the corresponding power imbalances, and applying the Linear Least Squares technique, the value of the inertia constant for each equivalent generator is approximated. In [19], PMU measurements are assumed to calculate the ROCOF after the disconnection of generation using a simple linear function within a given interval. The concept of the frequency of the center of inertia is considered in that case, along with the assumption that the related power imbalance of the event is completely known to estimate the equivalent inertia of the study system. By using the swing equation and kinetic energy principles, system inertia is approximated in [20] using power and frequency changes measured at generator buses following a given disturbance. In particular, inertia is evaluated there with the selection of the maximum value of resultant ROCOF and the determination of the corresponding change in power for each generator at that time instant. The overall process of these and other related approaches reported in the literature can be summarized as in Fig. 7. Either transient event measurements during inertial response or continuous ambient information is used in general, independently of the specific algorithms to approximate inertia (either for individual generators or the whole system).

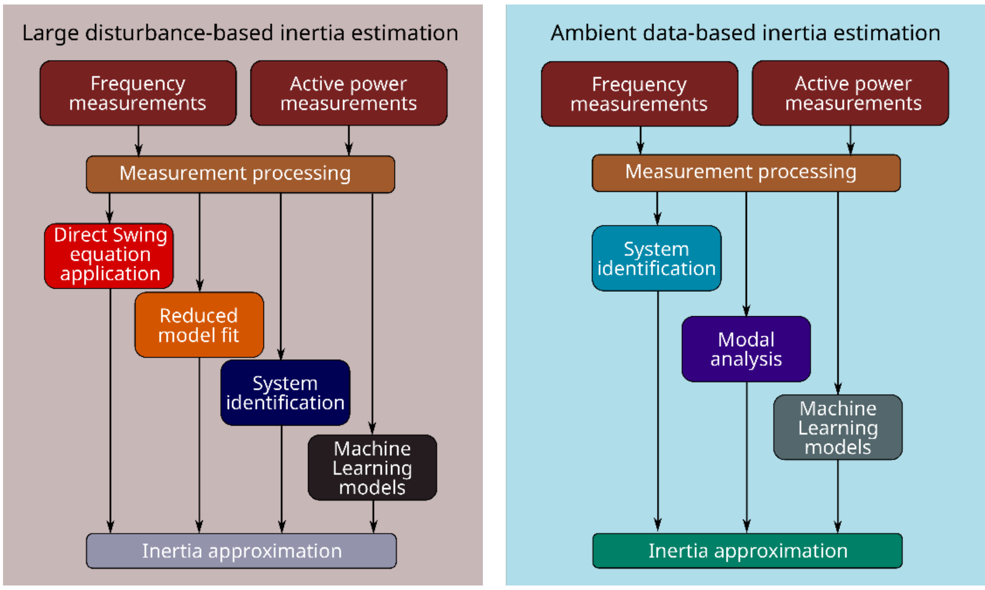

Fig. 7 Inertia estimation according to the source of PMU measurements.

Considering the given process associated with PMU measurements from transient events, the accuracy of both the ROCOF and power imbalance estimations has a significant impact on the computation of inertia. Different issues such as noise in measured signals, frequency spikes due to large disturbances, time delays because of filtering actions, deviations between rotor speed and generator terminal frequency, and correct detection of disturbance time instant, should be appropriately addressed to achieve a reliable calculation. Moreover, since transient events are typically very infrequent and the inertia can be computed only for the specific operational condition at the time of the event, this approach cannot be used for continuous monitoring purposes. On the other side, although the estimation of inertia using ambient measurements seems to be more suitable for this, minutes of data might be required to accomplish a successful identification of the considered dynamic model. Furthermore, the approximation of rotor speed with the terminal frequency of the corresponding generator bus could also lead here to significant errors.

The increasing collection of data with PMUs and the advancements in Machine Learning (ML) techniques has also opened up the application of different strategies from the data-driven perspective, as indicated in Fig. 7. Therefore, neural networks (NNs) with fully connected layers [21] for example, or even more advanced architectures [22], are proposed to assist the estimation of inertia. In [21], a multilayer perceptron (MLP) network was considered, and the inputs to the model were determined from a correlation analysis between power system variables that can be measured with PMUs and inertia. Then, the MLP network was trained using a dataset obtained from power flow simulations with the test system model using a commercial platform for power system analysis. In [22], more complex alternatives based on long-recurrent convolutional NNs and graph convolutional NNs are presented and, by assuming the availability of ambient measurements of speed deviation and its derivative at generator buses, the proposed architectures are trained to dynamically approximate the inertia of the test system. In general, the process involved in the development of a ML model using a NN approach can be illustrated as in Fig. 8.

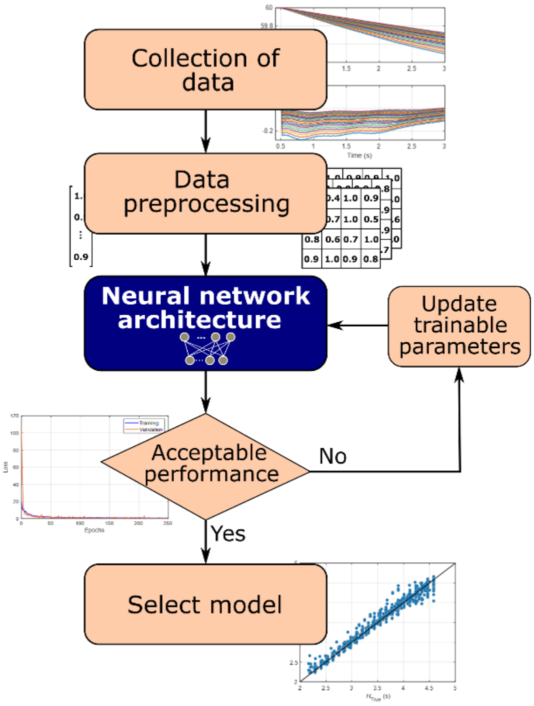

Fig. 8 NN model training and selection process.

As inferred from Fig. 8, a suitable and reliable dataset is necessary for training and building a model that can appropriately generalize to new and unseen information. Therefore, a relatively large and diverse set of representative samples must be available first. In general, real measurements are insufficient for this purpose since they normally cover only a few operating conditions and scenarios. Therefore, synthetic data are usually generated and considered to build or complement the dataset. Besides, after the training, testing and deployment of an acceptable model, continuous monitoring of its performance on live data and retraining are required to adapt to different data changes, and to ensure the quality of the model. Aforementioned issues related to raw measurements should also be tackled here, particularly when the ROCOF is selected as one of the inputs.

Based on offline data post-processing, three different approaches are illustrated next for the estimation of inertia.

2.2.1.1 Offline estimation of total inertia using an ARMAX model

The ARMAX (Autoregressive Moving Average with eXogenous input) model [23] is a system identification technique that can model the relationship between power system frequency and active power fluctuations. The general form of the ARMAX structure in the backward shift operator *q* is:

$$A(q)y(t) = B(q)u(t - n_k) + C(q)e(t) \tag{7}$$

where

$$A(q) = 1 + a_1 q^{-1} + \cdots + a_{na} q^{-na} \tag{8}$$

$$B(q) = b_1 + b_2 q^{-1} + \cdots + b_{nb} q^{-nb+1} \tag{9}$$

$$C(q) = 1 + c_1 q^{-1} + \cdots + c_{nc} q^{-nc} \tag{10}$$

and *y(t)* and *u(t)* are respectively the output and input at time *t*, *nk* denotes the input delay, *na*, *nb* and *nc* represent the order of polynomials *A(q)*, *B(q)*, and *C(q)*, a_is and b_is refer to the parameters to be identified, and *e(t)* stands for the noise term.

By using system identification techniques, the discrete-time dynamic model in (9) can be obtained from a complete batch of measured data within a predefined time window (non-recursive) [24]. Then, it can be converted to the continuous transfer function in (6) to extract the equivalent information related to the inertia constant.

The results of this approach are illustrated here through the simulation of the sample power system in Fig. 9. This test grid emulates the frequency dynamics of the physical four-machine system setup at the Renewable Electrical Energy Laboratory of ZHAW [25]. All synchronous generators (G_{11}, G_{12}, G_{21}, and G_{22}) are equipped with Automatic Voltage Regulators and speed governors. An initial condition where the generators in Area 1 are supplying 185 W and 180 W, and each one in Area 2 is providing 185 W to the system, was assumed. Besides, with the considered loads at buses 7 and 9, a total active power transfer of 64 W is established from Area 1 to Area 2.

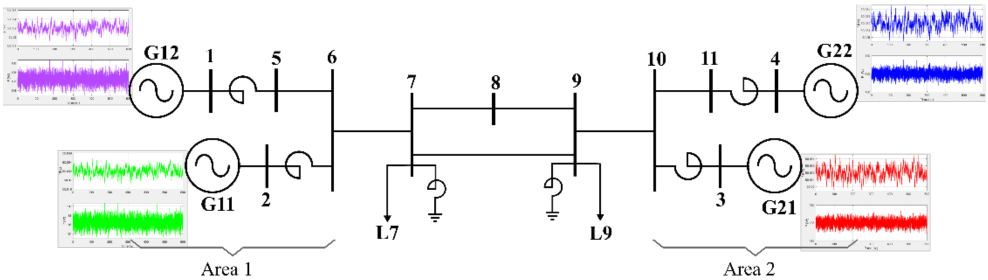

Fig. 9 Test power system.

By using a version of the simulation model in DIgSILENT PowerFactory [26], its capability to approximate the frequency dynamics of the physical setup is illustrated in Fig. 10, where the system response to a sudden step change of 32% in the active power of the load at bus 7 is depicted.

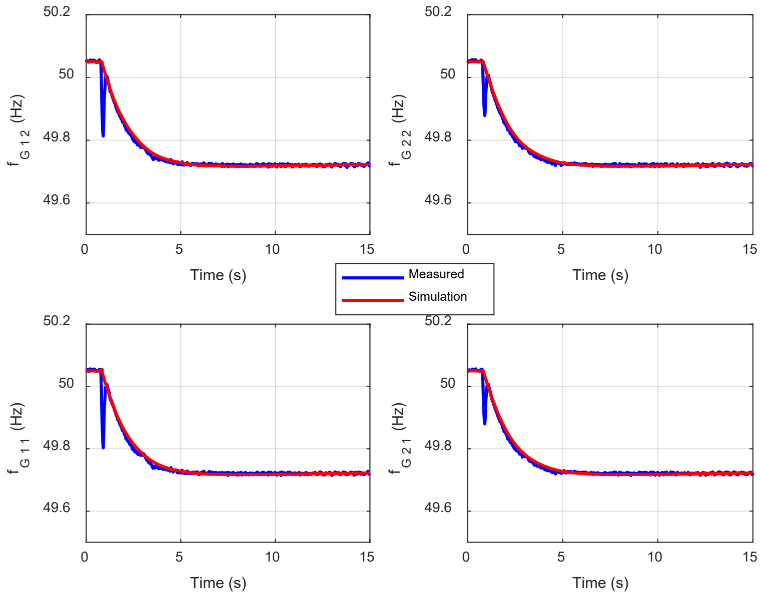

Fig. 10 System frequency response.

Now, for system identification purposes, Gaussian distributed noise with a zero mean value and known variance was added to the system through random variable loads at buses 7 and 9. With a sampling time of 0.02 s, a total of 30'000 data points from P_g and f_b measurements were collected for each generator and for different sets of machine inertia constants. The considered cases in this regard and the corresponding results of estimated system inertia ($\widehat{\boldsymbol{H}}_{sys}$) are given in Table 1.

Table 1. Offline estimation of inertia.

Case	Inertia constant (s)				|Error| (%)
	G_{11} & G_{12}	G_{21} & G_{22}	H_{sys}	$\hat{H}_{sys}$	
1	11.95	11.95	11.95	11.87	0.60
2	16.00	16.00	16.00	15.84	0.97
3	6.00	16.00	11.00	10.81	1.65
4	7.00	7.00	7.00	6.99	0.07
5	5.00	12.00	8.50	8.50	0.06
6	10.00	4.00	7.00	6.16	11.99
7	4.5	7.00	5.75	5.98	4.07

2.2.1.2 Offline estimation by direct use of the Swing equation

In this case, real measurements from a physical setup of the grid in Fig. 9 are used, where the system response under a step load change at bus 7 is considered. Based on (3), the computation of the equivalent system inertia (H_T) is carried out here by taking into account the net power imbalance ΔP_T (immediately after the disturbance) and the ROCOF at 500 ms (from the frequency of the center of inertia f_{coi}), where:

$$H_T = \frac{\Delta P_T}{2 \cdot \frac{df_{coi}}{dt}} \frac{f_0}{S_B} \tag{11}$$

and,

$$f_{\text{coi}} = \frac{\sum_{i=1}^{G} H_i \cdot S_{ni} \cdot f_i}{\sum_{i=1}^{G} H_i \cdot S_{ni}} \tag{12}$$

Considering the resultant system dynamics in terms of f_{coi}, as shown in Fig. 11, the approximation of the ROCOF (red dotted line) at 500 ms turns out to be -0.18376 for a ΔP_T =-395 W. Then, by using (11), the estimated value for H_T is 16.8 s. However, this quantity significantly differs from the true value, which is supposed to be around the one indicated for Case 1 in Table 1. Corresponding computations were also carried out with the available simulation model of the system and the predefined disturbance, and the estimated value was 16.4 s. The deviations in both cases have to do with the approximation of the ROCOF based on the frequency response and the time instant of the perturbation, which can clearly lead to significant errors.

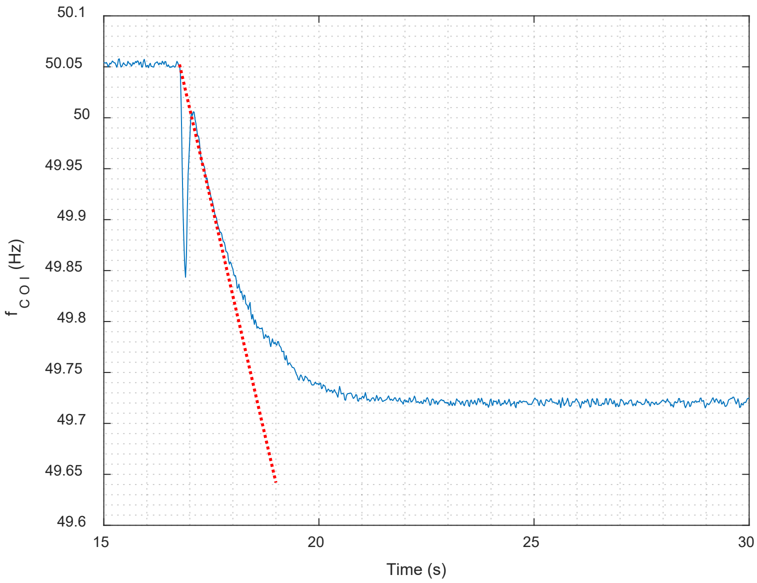

Fig. 11 System response after disturbance.

2.2.1.3 Application of a convolutional neural network (CNN) approach

Since advanced ML algorithms are currently opening new avenues and possibilities for better predictions and analysis in ever more increasingly complex tasks, alternatives based on these approaches are also being investigated for inertia estimation applications. The example illustrated here is based on [27], where a CNN architecture is used to determine the equivalent inertia of a 39-bus benchmark system under low-inertia scenarios. The CNN model was trained in a supervised way with a set of input-output examples composed of the frequency of the center of inertia, corresponding computed rates of change of frequency, and target inertia values. Input data were collected from the simulation of sudden generation outages and load step changes under variations of total load demand and modifications in the equivalent inertia of the base system. After training, a new and unseen set of data was used to test and evaluate model's performance, and the results of the estimated inertia, as compared to the true values, are illustrated in Fig. 12.

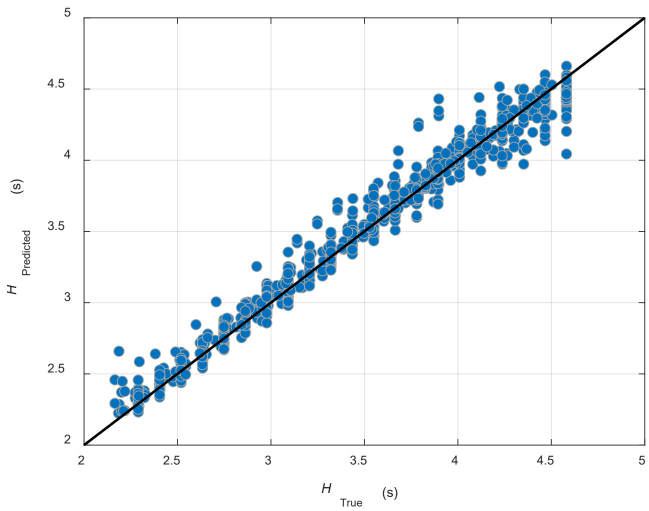

Fig. 12 Predicted vs. actual inertia values.

Considering the coefficient of determination R^2, as a measure to quantitatively determine the corresponding accuracy of the model:

$$R^2 = 1 - \frac{\sum_{i=1}^{n_{samples}} (y_i - \hat{y}_i)^2}{\sum_{i=1}^{n_{samples}} (y_i - \bar{y})^2} \tag{13}$$

where y_i represents the target value, $\hat{y}_i$ refers to the model prediction, and $\bar{y}$ indicates the mean value of the desired outputs, then the results in Table 2 were obtained, where two traditional machine learning techniques, such as Support Vector Machine (SVM) and Random Forest, were additionally included for comparison purposes.

Table 2. R^2 results for the test set.

Model	R^2
CNN	0.978
SVM	0.950
Random Forest	0.907

2.2.2 Dynamic monitoring of inertia

According to the analysis of alternative algorithms for the estimation of system inertia through PMU measurements in Section 2.2.1, and the results of the described examples, an ARMAX based method was selected for further investigation. However, the non-recursive method calculates the ARMAX model parameters using all available data simultaneously in one single operation. Therefore, it cannot be used for online and continuous monitoring to track changing system dynamics over time. In addition, to avoid the limitations of different approaches completely dependent on the occurrence of system frequency events (large power imbalances), ambient measurements were considered here together with recursive ARMAX approximation [23], [24]. The adopted alternative, the study system and data generation for testing purposes, the achieved results from offline estimations, as well as the online implementation and performance of the algorithm in real-time, are described in the following subsections.

2.2.2.1 Recursive ARMAX with forgetting factor

A recursive estimation method that updates the model parameters sequentially as each new data point arrives is selected in this case. The ARMAX model structure is the same as the one described by (7)-(10). To prevent old data from dominating new updates, a forgetting factor λ is used to exponentially weight recent data more heavily. Then, based on previous parameters estimates, new parameters are calculated according to the following adaptation process [23], [24]:

$$\hat{\theta}(t) = \hat{\theta}(t-1) + K(t)[y(t) - \hat{y}(t)] \tag{14}$$

$$\hat{y}(t) = \psi^T(t)\hat{\theta}(t-1) \tag{15}$$

$$K(t) = \frac{P(t-1)}{\lambda + \psi^T(t)P(t-1)\psi(t)}\psi(t) \tag{16}$$

$$P(t) = \frac{1}{\lambda}\left[P(t-1) - \frac{P(t-1)\psi(t)\psi^T P(t-1)}{\lambda + \psi^T(t)P(t-1)\psi(t)}\right] \tag{17}$$

where $\hat{\theta}(t)$, $y(t)$ and $\hat{y}(t)$, are the model parameter estimate, the observed output, and the prediction at time *t*, respectively, *K(t)* denotes the gain that weights the current prediction error on the parameter update, $\psi(t)$ is the regressor vector, and *P(t)* refers to the covariance matrix.

2.2.2.2 Offline inertia estimation with recursive ARMAX

By considering the same power system model represented in Fig. 9, a simulation of 700 s was executed, where diverse inertia values for Area 1 (A1) and Area 2 (A2) at different periods of time were assumed. With the collection of active power and frequency at generation buses at every 20 ms, a dataset composed of 35’000 data points was built. The estimation of the equivalent system inertia in this part of the study was addressed by approximating first the inertia of each area, and then combining this information appropriately.

By using MATLAB [28], the active power and frequency deviations in A1 and A2 were first preprocessed by signal lowpass filtering and then removal of means values. According to this, Fig. 13. shows the obtained information after that.

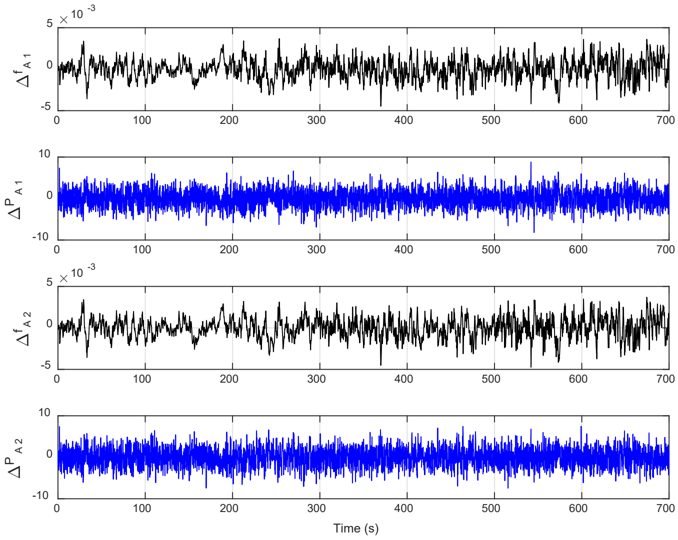

Fig. 13 Information for inertia estimation.

For the appropriate identification of the systems characterized by the dynamics in Fig. 13, several orders for the parameters and delay in (7)-(10) were tried. Then, after extensive model performance analysis, an ARMAX model with $n_a = 1$, $n_b = 2$, $n_c = 1$, and $n_k = 1$ was determined. Considering the estimation of time-varying coefficients, a forgetting factor of 0.99 was stablished to decrease the influence of past samples. The fitting results of the selected model are presented in Fig. 14 for a particular data interval, where a relatively good fit between the reference signal and the output from the ARMAX model can be inferred. On the other side, the convergence of the estimated parameters for the different inertia changes contained in the information from Fig. 13 is illustrated in Fig. 15 (through the coefficients of the polynomials A and B).

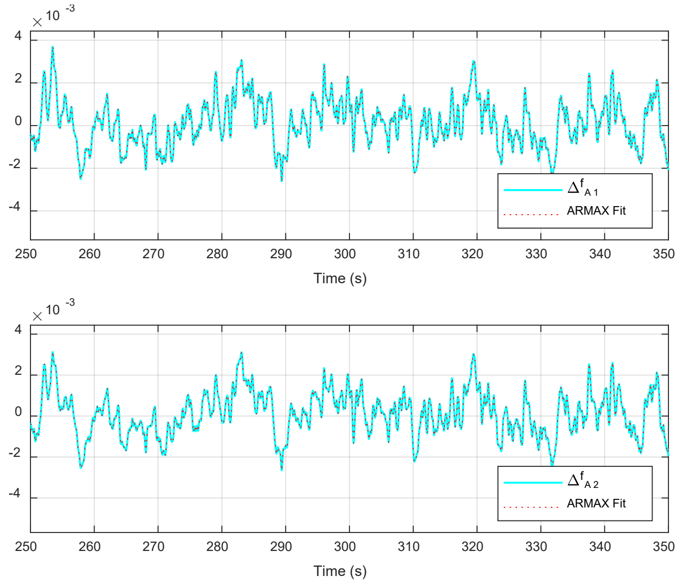

Fig. 14 Fitting of the selected ARMAX model for A1 and A2.

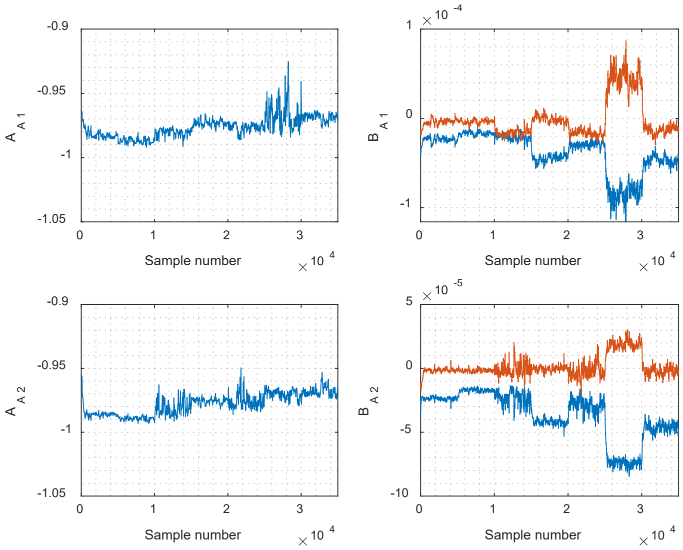

Fig. 15 Estimated parameters for polynomials A and B.

By fitting the output of two ARMAX models as exemplified in Fig. 14, and using the estimated parameters that characterize the incoming inputs and outputs in Fig. 13, the inertia of each area was separately estimated and then combined and processed to approximate the equivalent inertia of the whole system. The results of this computation are illustrated in Fig. 16, where the estimated values (red curve) are compared to the actual inertia of the study grid (green curve). As it can be deduced from these results, the considered ARMAX models can quickly track the assumed changes and provide a means to continuously approximate the inertia of the system around the true values.

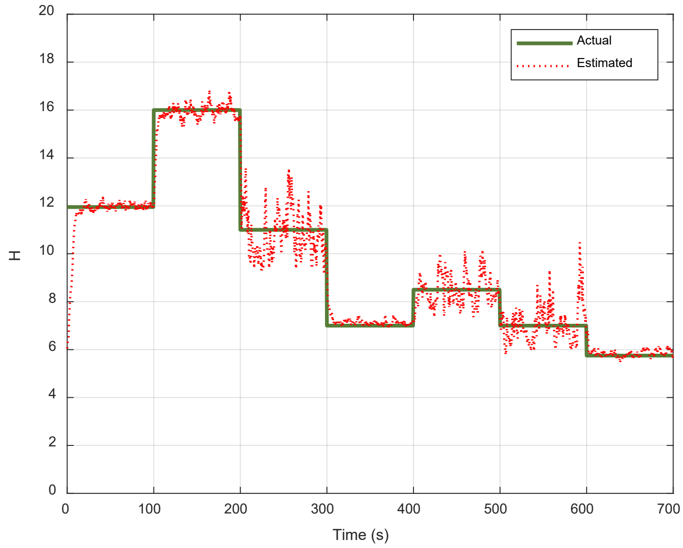

Fig. 16 Equivalent system inertia (offline and recursively).

2.2.2.3 Online and real-time inertia estimation

After extensive offline performance evaluation in Section 2.2.2.2, further investigations were carried out in an online and real time manner. To be able to accomplish this, the version of the test power system model in DIgSILENT PowerFactory was exported to PSS/E format and then adapted for its execution in a real-time simulation environment through OPAL-RT's ePHASORsim [29]. Besides, the considered algorithm for inertia estimation was then deployed and configured through Simulink blocks [28]. A general illustration of the involved implementation in the ePHASORsim tool is shown in Fig. 17.

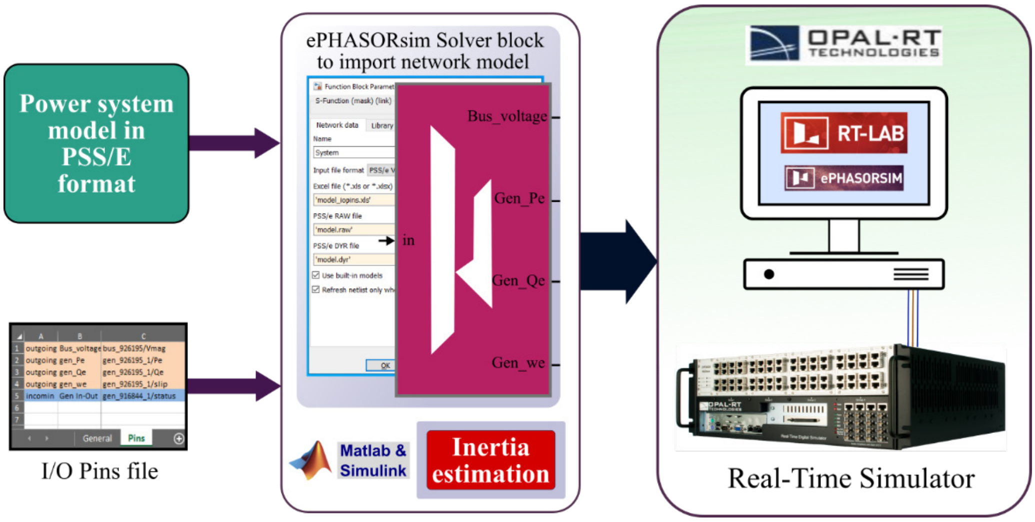

Fig. 17 Real-time implementation setup.

Regarding the "Inertia estimation" block highlighted in Fig. 17, an overall overview of its content is provided in Fig. 18. As illustrated, a Recursive Polynomial Model Estimator was configured and used as an ARMAX model structure to estimate the polynomial coefficients required to extract the inertia values from the given signals. The arrangement in Fig. 18 can be used in general to approximate either the inertia of a particular generator, the inertia of a given system area, or the overall inertia of the test network (depending on the points of measurement and the way they are combined).

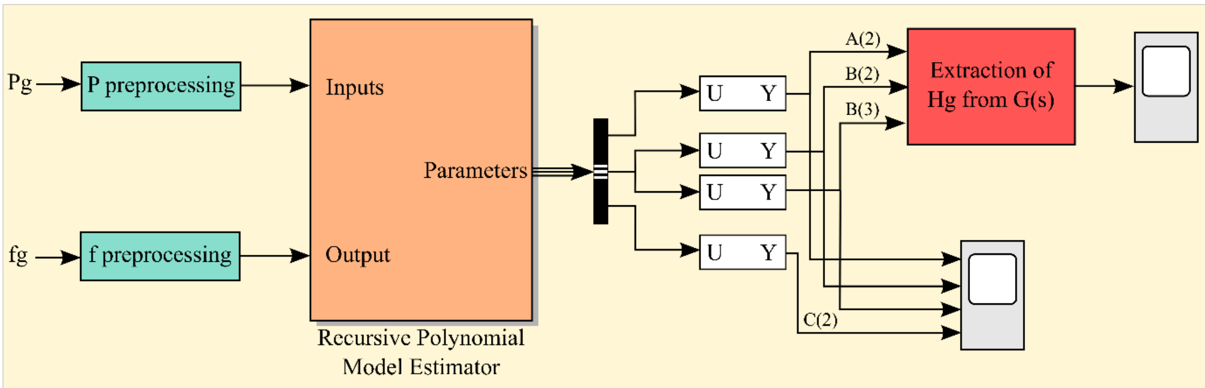

Fig. 18 Inertia estimation algorithm in Simulink.

For performance evaluation purposes, different study cases were defined and implemented according to the generator and system inertia variations given in Table 3.

Table 3 Case studies for online inertia estimation.

Case	**Inertia constant (s)**				
	G_{11}	**G_{12}**	**G_{21}**	**G_{22}**	**Hsys**
i	12.0	7.0	9.0	4.0	8.00
ii	12.0	16.0	14.0	10.0	13.00
iii	7.0	4.5	8.0	6.0	6.37
iv	4.0	11.0	8	12.0	8.75

Then, by applying the scheme in Fig. 18 to determine the inertia of each individual generator, the results in Figs. 18 to 21 were achieved, where the solid line curves denote the estimated values at every sampling interval (10 ms here) and the dotted lines represent the true inertia constants. As it can be observed from these figures, the estimated inertias closely convergence to the true quantities (in around 25 s after initiating the identification process) and afterwards they fluctuate slightly around the actual values. By using these estimations to approximate the equivalent inertia of the system at any given instant, the results indicated by the solid green curve in each case were obtained.

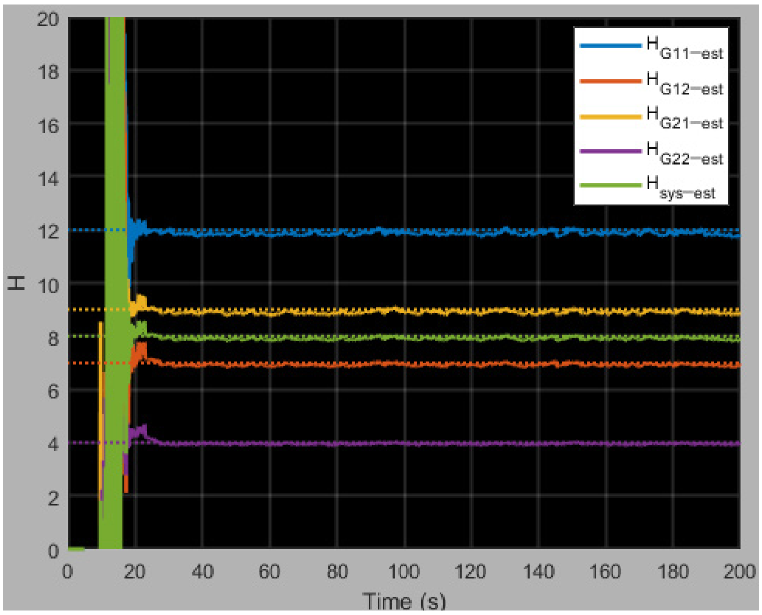

Fig. 19 Results for Case i.

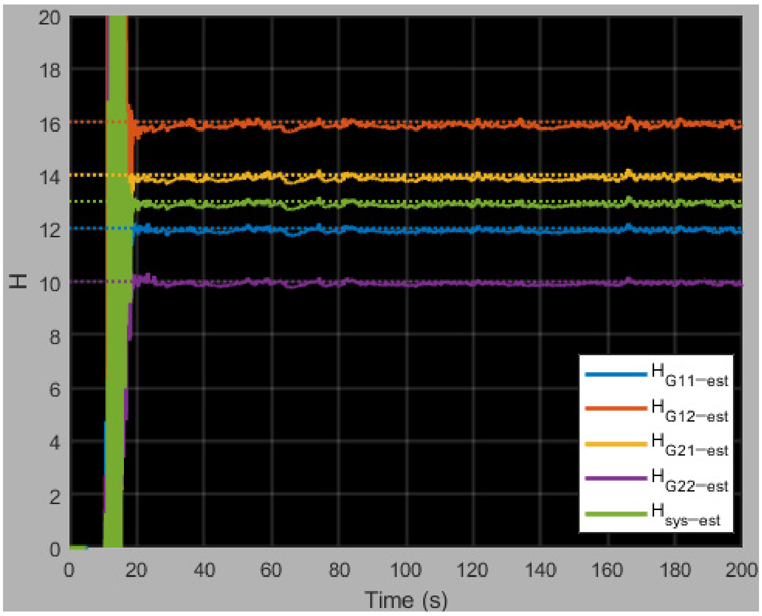

Fig. 20 Results for Case ii.

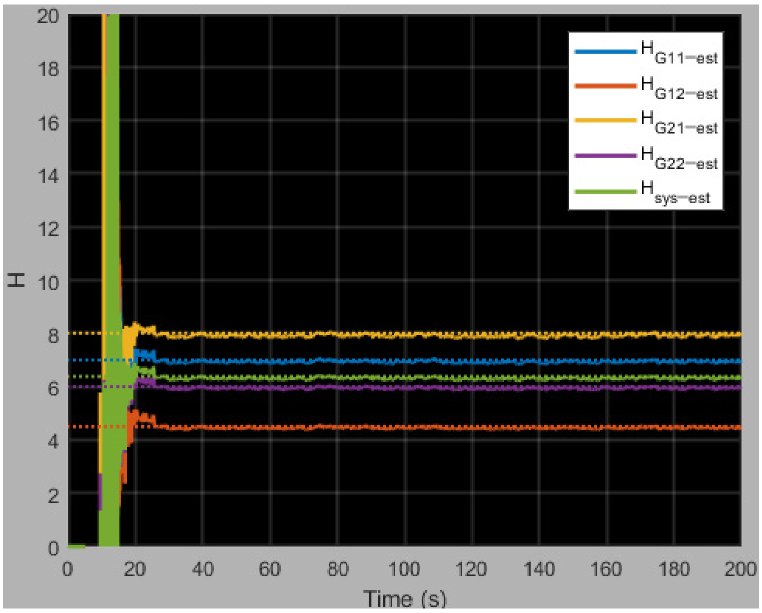

Fig. 21 Results for Case *iii*.

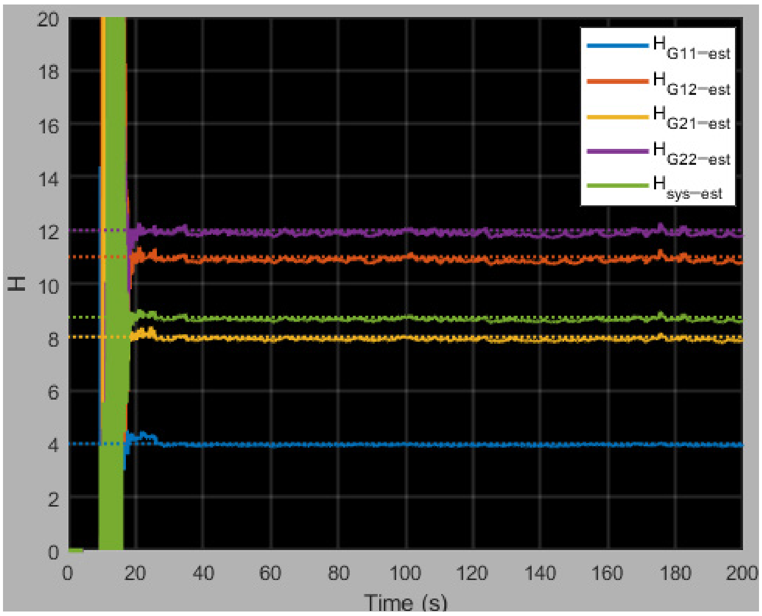

Fig. 22 Results for Case *iv*.

Further studies were performed with the specifications for Case *iv* in Table I. In this regard, Fig. 23 shows the results associated with equivalent inertia of the system when the generator G_{11} is suddenly disconnected from the grid at 200 s. As observed from this test, the estimations work quite well before the disturbance produced by the tripped generator, since a clear convergence to the true values can be perceived. After the assumed abrupt change, a certain deviation from the new actual value can be noticed, although the attained difference is relatively small and can be acceptable. For illustration purposes, the convergence of the estimated parameters for the identified model related to G_{11} in Case *i*, and to G_{12} in Case *iv*, is exhibited in Fig. 24 for the coefficients of polynomials A and B.

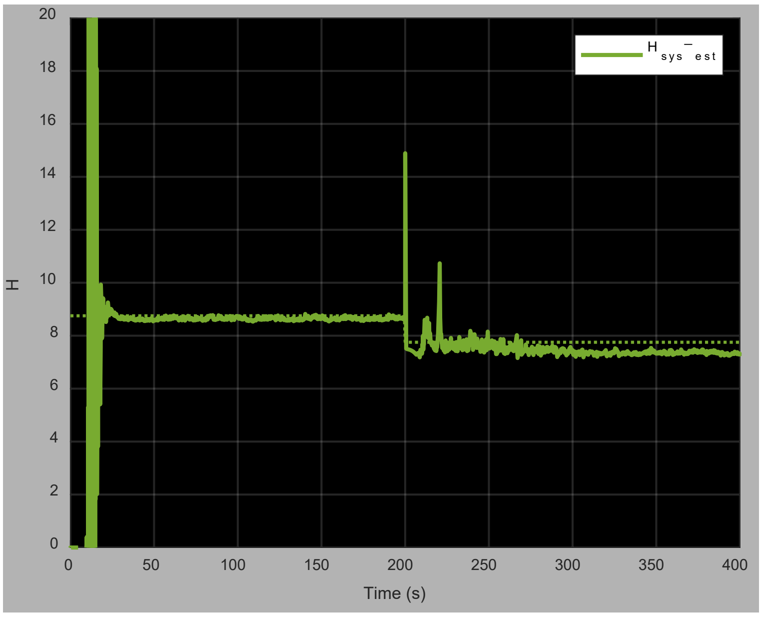

Fig. 23 Results for Case iv with trip of G_{11} at 200 s.

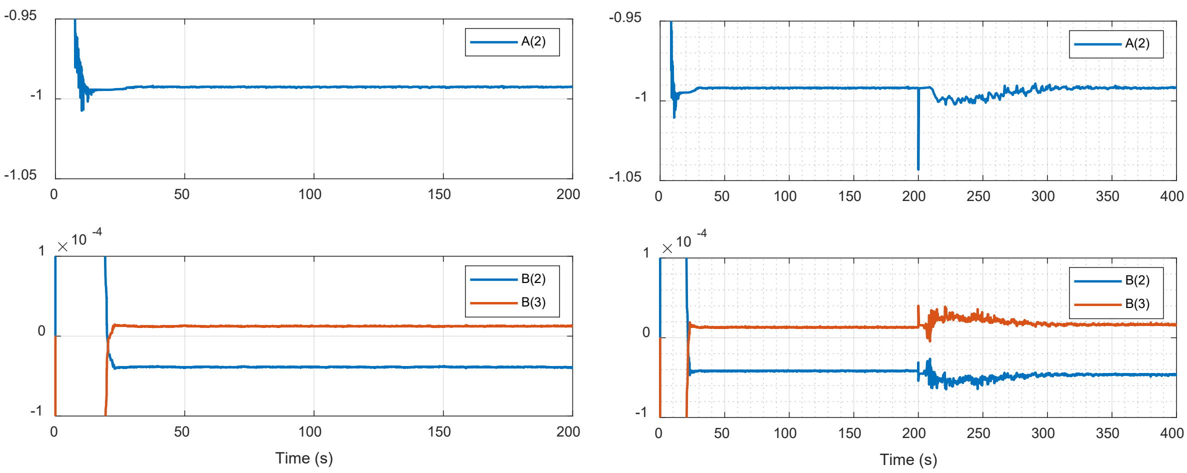

(a) (b)

Fig. 24 Estimated parameters related to (a) G_{11} in Case i, and (b) G_{12} in case iv.

2.2.2.4 Real-time inertia estimation with ARMAX, ARX and OE models

The studies from the previous Sections are extended here with a larger test grid (as compared to the one in Fig. 9), and the ARX and OE model structures (in addition to ARMAX). The sample power system in this case is represented inf Fig. 25, which is composed of three transmission zones and portrays an isolated electrical grid.

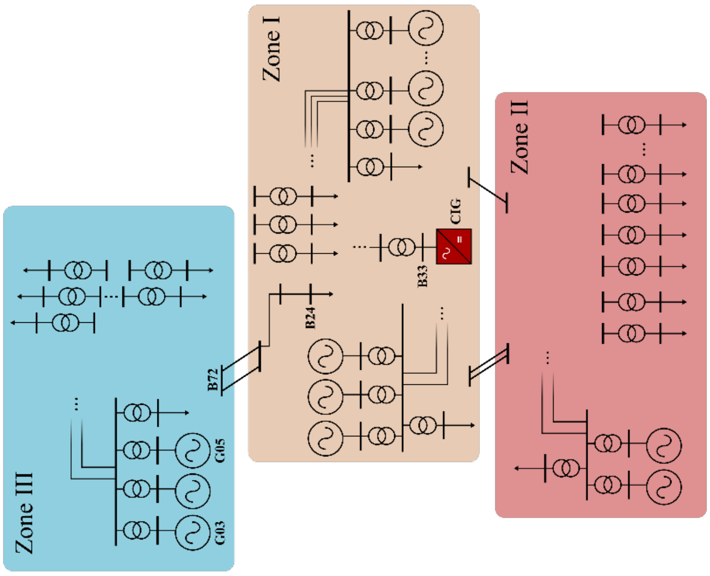

Fig. 25 Representation of the sample power system.

Now, for time-domain simulations, a model encompassing the representation of 74 buses, 13 synchronous generators, one Converter-Interfaced Generation unit, 30 loads, 50 lines, and 48 transformers was assumed. All synchronous generators are equipped with governors to mimic frequency regulation and managing of active power supply.

Regarding the two additional discrete models for system identification, the ARX (Auto-Regressive with eXogenous Input) structure is given in the following [23], [24]:

$$A(q)y(t) = B(q)u(t - n_k) + e(t) \tag{18}$$

with *A(q)* and *B(q)* as in (8)-(9). It is a simple model that can be computationally efficient due to a linear least square solution. However, the shared coefficients of the *A(q)* polynomial with both system and noise dynamics might lead to potentially biased parameter estimates in noisy environments.

On the other hand, the OE (Output Errror) model is given by the following expressions:

$$y(t) = \frac{B(q)}{F(q)}u(t - n_k) + e(t) \tag{19}$$

with

$$F(q) = 1 + f_1 q^{-1} + \cdots + f_{nf} q^{-nf} \tag{20}$$

and *B(q)* as in (9). As compared to ARMAX and ARX, this model is the simplest in terms of structure, as it only models the system's deterministic input-output relationship, treating the disturbance as purely measurement noise added at the output. However, its restrictive noise consideration often leads to less accurate or poorly estimated results.

ARMAX, ARX, and OE models were implemented in real-time to assess their performance in estimating inertia. In particular, the response of the algorithms is illustrated here by the approximation of the inertia constant of generator G05 in Fig. 25. Different system events are considered for this purpose, according to the study cases provided next.

Case i: No fault operating condition

With the system driven only by random noise, the dynamics of the active power and frequency from synchronous generators (P_{gs} and f_{gs}) is shown in Fig. 26 and Fig. 27. After activating the estimation algorithms at 20 s, they are used to approximate the inertia of machine G05. Achieved estimates are shown in Fig. 28, where the green dash-dotted line represents the true value.

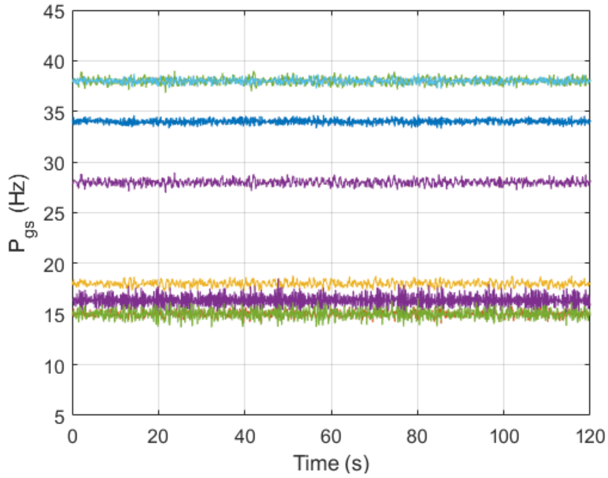

Fig. 26 Case *i*: Active power of SGs.

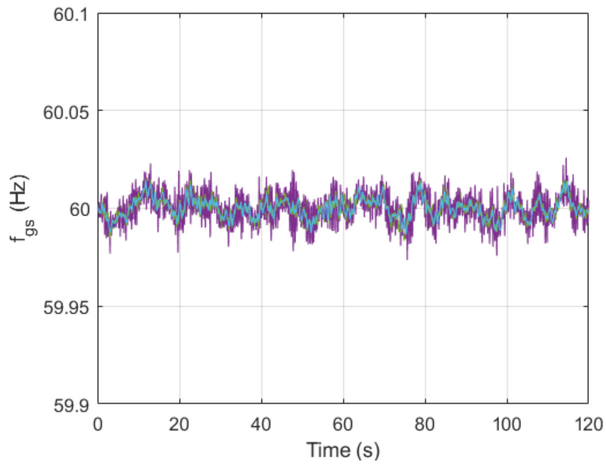

Fig. 27 Case *i*: Frequency of SGs.

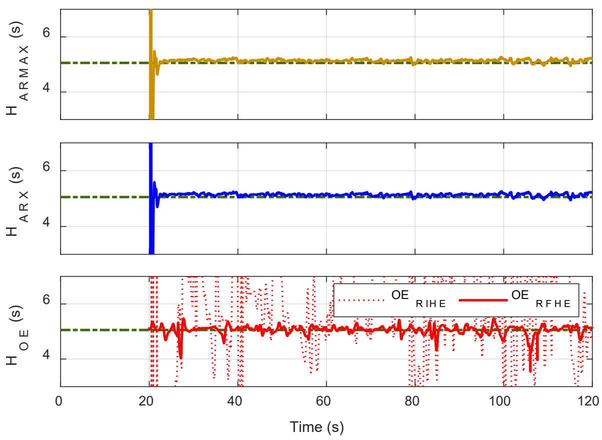

Fig. 28 Case *i*: Estimated inertia values.

As noted in the two upper subplots of Fig. 28, the ARMAX and ARX approaches immediately yielded acceptable results. In contrast, the recursive OE algorithm initially showed an erratic response, represented by the red dotted line in the corresponding subplot. Consequently, an RFHE alternative using a 200-sample sliding window was considered for the OE model. The results of this modification, illustrated by the red solid line in the same figure, show that the OE model was now able to provide better approximations. However, the ARMAX and ARX options still provided values that were closer and more consistent with the actual inertia. While the default settings of model parameters caused significant, transient variations immediately after the activation of the ARMAX and ARX approaches, these variations quickly reached relatively small values.

Case ii: Step change in Load

A 140% step increase was applied to the load connected at bus B24 in Fig. 25 at 50 s. The generators' output and frequency, produced by the event, are illustrated in Fig. 29 and Fig. 30. On the other hand, the corresponding inertia estimates are shown in Fig. 31. The considered load change causes a slight transient deviation in the estimated inertia from the ARMAX and ARX algorithms. However, after approximately 8 s, the estimations follow again the true value closely. On the other side, the estimates from the OE approach are in general more susceptible to the load disturbance, as observed from the significant variations appearing immediately after the applied perturbation.

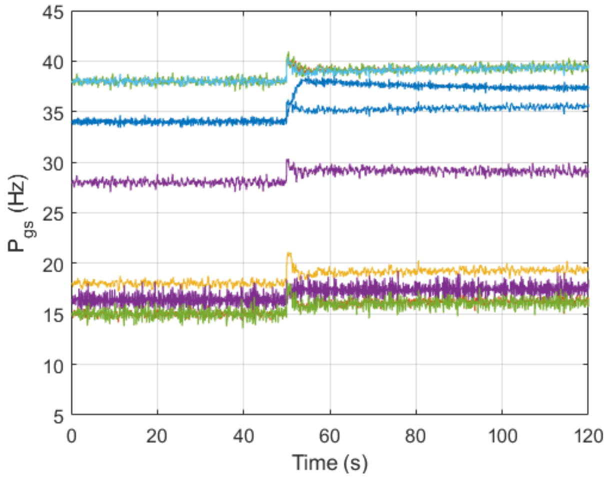

Fig. 29 Case *ii*: Active power of SGs.

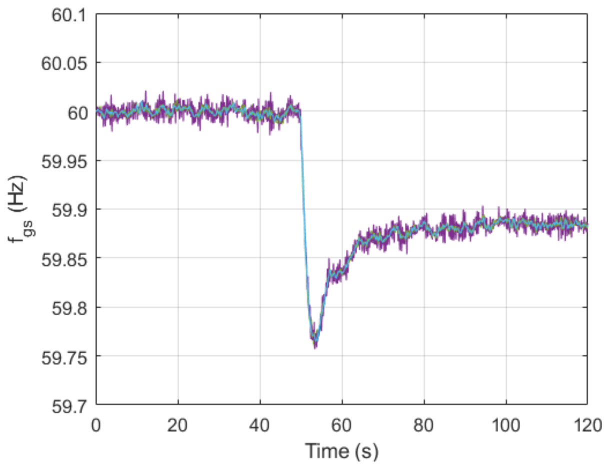

Fig. 30 Case *ii*: Frequency of SGs.

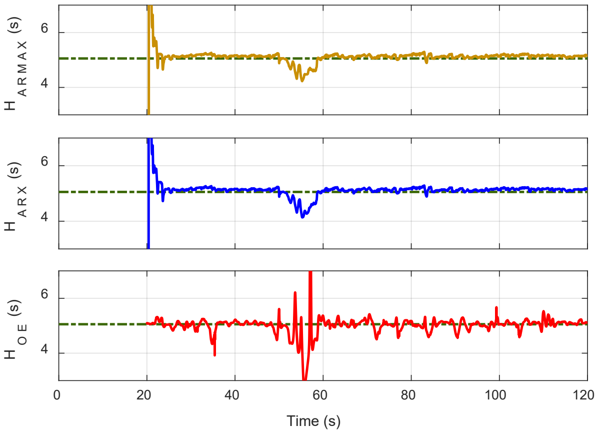

Fig. 31 Case *ii*: Estimated inertia values.

Case iii: Trip of generator

In this case, generator G03 in Zone III is tripped at 50 s. Due to the resultant active power imbalance, the frequency drops, but it is then restored to a new quasi steady-state operating point by primary frequency control. The corresponding dynamics of the grid are illustrated in Fig. 32 and Fig. 33. By using this information for the involved generator, the response of the implemented estimation algorithms is illustrated in Fig. 34. As it can be deduced, the ARMAX and ARX alternatives provide relatively accurate approximations even in the presence of the applied perturbation. On the contrary, the evaluations of the OE model deviate notably from the reference value, which tend to be in general more inconsistent.

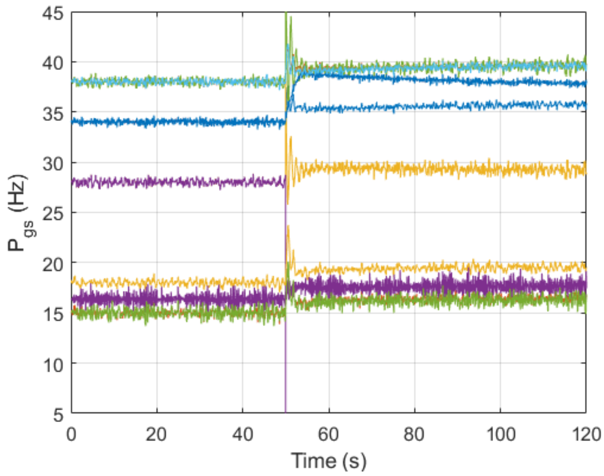

Fig. 32 Case *iii*: Active power of SGs.

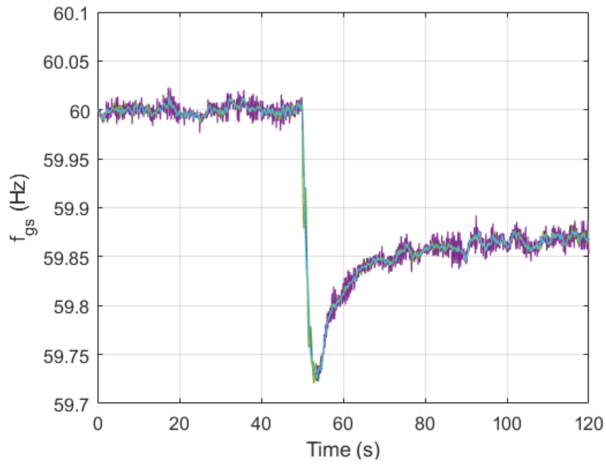

Fig. 33 Case *iii*: Frequency of SGs.

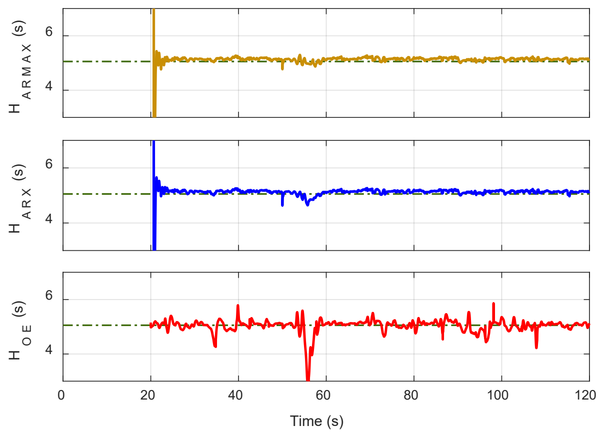

Fig. 34 Case *iii*: Estimated inertia values.

Case 4: Three-phase fault and line trip

Here, a three-phase fault is applied at bus B72 in Fig. 25 at 50 s, and then released by tripping one of the transmission lines between Zones III and I at 50.1 s. The active power and frequency response from synchronous generators in this case is shown in Fig. 35 and Fig. 36. As inferred, after the transient acceleration of the machines and clearing of the fault with the disconnection of one of the lines, a new equilibrium condition is reached. The resultant inertia estimates during the considered period of observation are exhibited in Fig. 37. As observed, an outstanding performance is provided by the ARMAX model, since the involved estimations are basically unaffected by the assumed perturbation.

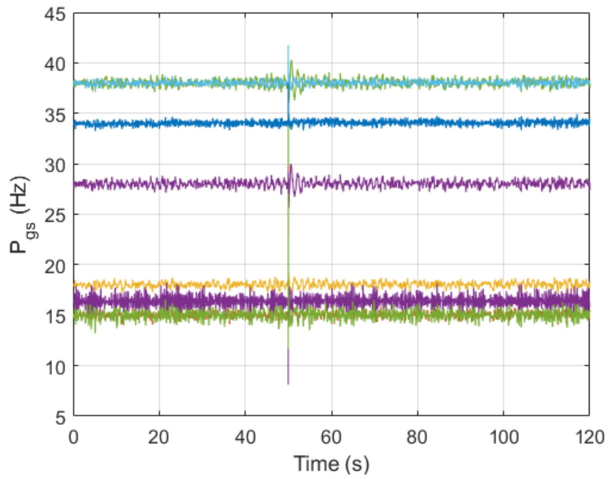

Fig. 35 Case *iv*: Active powers of SGs.

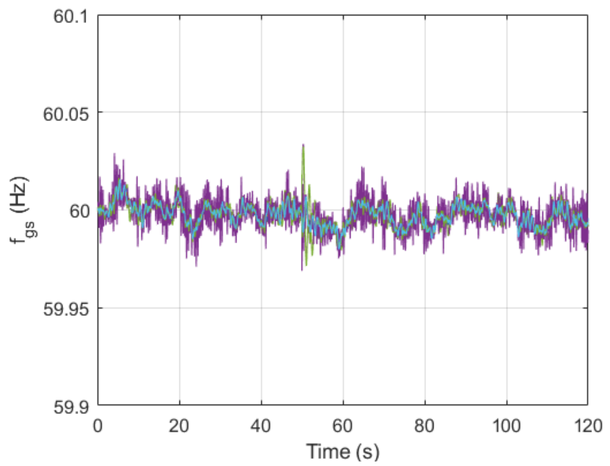

Fig. 36 Case *iv*: Frequency of SGs.

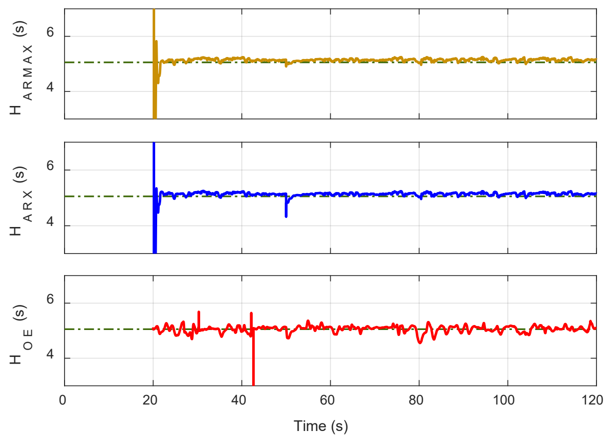

Fig. 37 Case *iv*: Estimated inertia values.

2.2.2.5 Real-time estimation of virtual inertia contributions

In order to assess the capability of different regression algorithms in identifying virtual inertia contributions, the CIG unit in Fig. 25 was enabled with Virtual Synchronous Machine (VSM) control. For this purpose, the simulation model illustrated in Fig. 38 was considered [30], where the related virtual synchronous generator is basically composed of an energy source, the converter, and a control mechanism. In particular, an ideal DC source is assumed to power de DC link, while an LC filter is included to implement the inverter's grid-side connection. The three-phase network is represented at this point by AC sources and associated resistances and inductances.

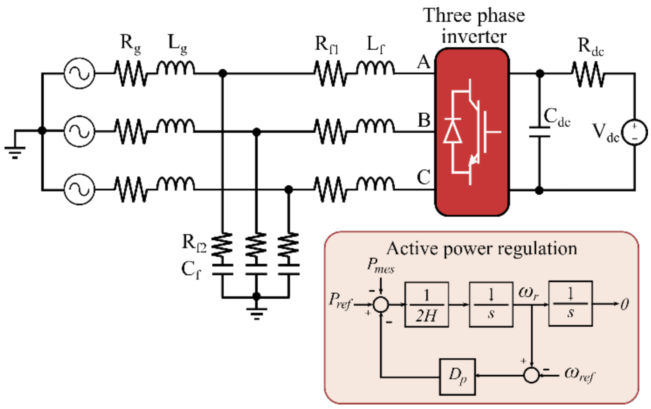

Fig. 38 CIG with VSM control.

Although the converter control part involves active and reactive power regulation loops, only the one related to active power control is represented in Fig. 38 for the specific purposes here. This loop mimics the dynamic behavior of a synchronous generator as related to the swing equation, with H being the inertia constant, P_{ref} the reference active power, P_{mes} the actual measured power, D_p the damping factor, ω_r and ω_{ref} the generated virtual and speed reference, and θ the associated phase angle. The inverter's PWM reference signals are generated via the voltage of the DC link, the angle obtained from reactive power control, and required sine transformations [30].

Based on Fig. 38, the VSM based CIG (VSM-CIG) was first implemented in Simulink and then its performance was initially validated independently. The response of the converter in this case is illustrated through modifications of H on one hand, and changes in the frequency of the AC voltage sources on the other hand. Fig. 39 depicts the behavior of the active power supplied by the inverter with different values of the moment of inertia $M=2H$. In every example, a step change in the reference active power from 5 kW to 10 kW was applied at 4 s. The considered integration step size for the simulations was 250 µs. The effect of different values for M can be seen through the resultant oscillations in the active power response, as well as the time to reach the new steady-state condition.

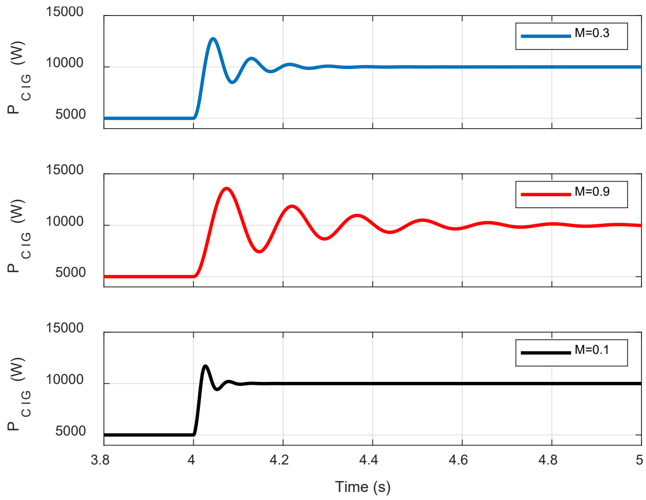

Fig. 39 Active power transient response for different values of *M*.

On the other side, the ability of the inverter to provide frequency support is depicted in Fig. 40. For simplicity, the nominal frequency of the AC voltage sources in Fig. 38 was directly changed at 4 s, while keeping *M* in the VSM control constant. For illustration purposes, step changes of -0.05 Hz and +0.03 Hz were separately applied. According to this, Fig. 40 shows how the converter increases or decreases the supplied active power based on the assumed frequency changes.

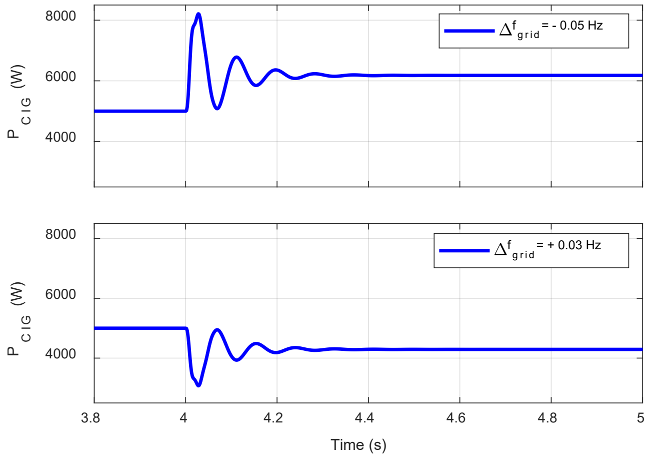

Fig. 40 Active power transient response to changes in Δf_{grid}.

After the independent assessment of the VSM-CIG model, it was integrated into the dynamics of the test power system in Fig. 25. The real-time implementation setup for the evaluation of selected algorithms in estimating virtual inertia is summarized in Fig. 41.

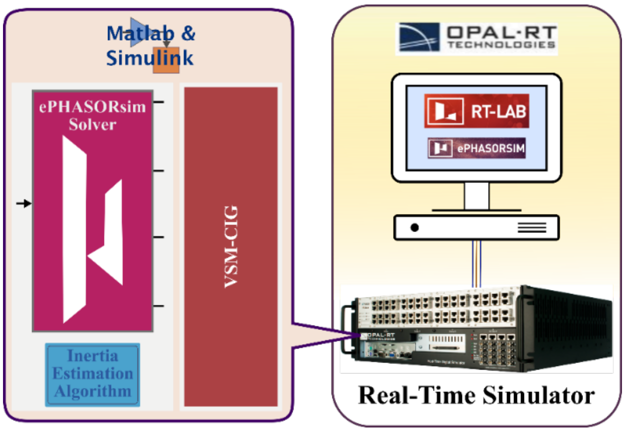

Fig. 41 Real-time deployment.

The data files of the test power grid are supplied through the ePHASORsim solver mask. Inertia estimation algorithms were implemented via Simulink. Besides, while the power grid model and inertia estimation run in phasor domain, the VSM-CIG runs in EMT domain. The general interaction and exchange of information here between phasor and EMT domains is illustrated in Fig. 42.

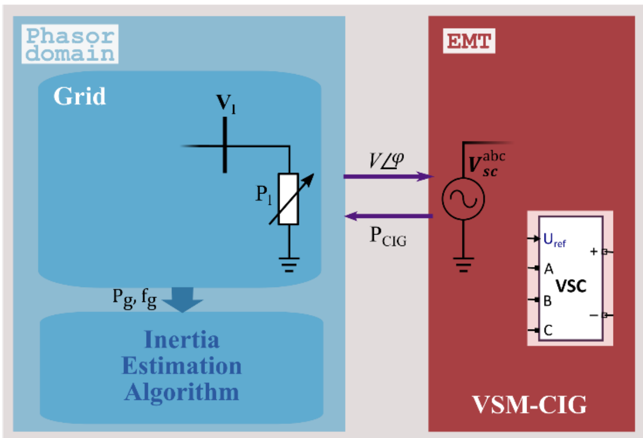

Fig. 42 Established interaction between phasor and EMT domains.

Because of the better performance shown by ARMAX and ARX models in the previous sections, as compared to the OE structure, both of them were investigated here to quantify virtual inertia contributions. In this regard, the parameter H of the VSM-CIG was assumed to be the target to be approximated by such estimation algorithms. The estimation performance in this case is illustrated by step changes in H from 0.3 to 0.9 at 45 s, then to 0.45 at 70 s, and finally to 0.7 at 95 s. The order of the models was selected as na=1, nb=2, and nc=1 for the ARMAX structure, and as na=1 and nb=2 for the ARX model. Fig. 43 illustrates the inertia estimates with a forgetting factor of 0.990 in both algorithms. As it can be deduced, the implemented alternatives were able to quickly adapt to changes and continue to provide relatively accurate approximations. It was possible to achieve an even more stable and smoother response by setting λ to 0.995, as illustrated in Fig. 44. However, despite the lower variance of the estimates, the tracking capability becomes a little bit slow. So, there is a trade-off between fast adaptation to changes and robustness against noise and steady-state accuracy. In any case, Fig. 43 and Fig. 44 show that the time-varying contributions of virtual inertia (from the assumed CIG unit with VSM) can be effectively tracked in real-time. By considering measurements from a common interconnection bus in the grid, the approach can be applied to approximate the equivalent virtual inertia either of a single unit or a group of CIGs.

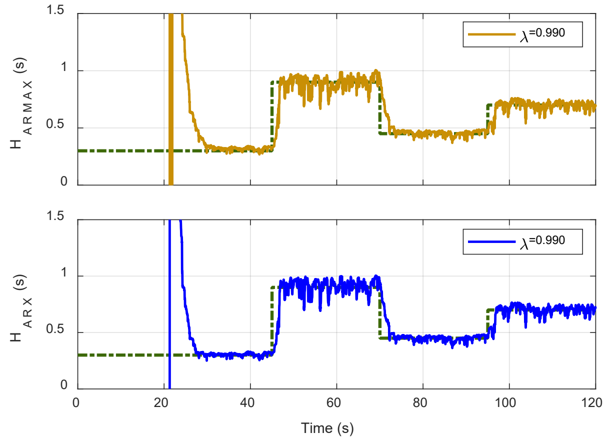

Fig. 43 Estimated virtual inertia with ff=0.990.

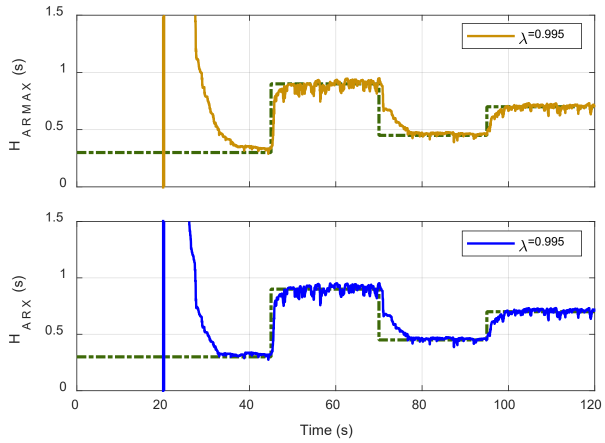

Fig. 44 Estimated virtual inertia with ff=0.995.

3 Conclusions and outlook

In general, with the large-scale integration of CIG and replacement of SGs, the total physical inertia of the system declines and the grid frequency changes more rapidly following a disturbance. Besides, the equivalent inertia of the grid is no longer a relatively constant value, since it changes dynamically according to the number of SGs online and the output of varying renewable energy. Under this scenarios, continuous monitoring of inertia is essential for system operators to maintain the reliability and security of operation. However, due to the high proliferation of inverter-based resources and increasing contamination with spurious interferences, new measurement procedures and instruments are necessary for the accurate tracking of fundamental frequency and ROCOF. According to the results of this project, the following main conclusions can be derived:

- To the state of the art, PMUs represent the most accurate solution to capture frequency and power deviations in all nodes of interest. The performance required by the reference standard is not sufficient to attain the desired level of accuracy and responsiveness. In particular, it is important to improve the performance in the presence of high distortion rates and fast dynamics. In this project, this has been obtained by using a Taylor-Fourier Multifrequency model. This demonstrates how it is possible to improve significantly the PMU performance by keeping a typical hardware architecture (in terms of ADC and clock) while increasing the complexity of the signal model and processing.

- By definition, PMUs provide local measurements which are referred to a single node of the power system. However, inertia is a system parameter and cannot be properly identified only at a local level. It is necessary to merge the measurements together, either by traditional state estimation and power flow techniques or by defining new aggregation techniques. In particular, it is important to develop criteria for the definition of regional metrics. This is straightforward for the power exchange between one portion and another of the power system, whereas it is more complicated for the frequency variations. In this project, the theory of control cards has been used to develop flexible criteria for the aggregation of frequency and ROCOF measurements from close-by nodes. This proves beneficial in two aspects. First, it reduces the effect of noise on derivative measurements. Second, it simplifies the model of the power system under analysis.
- It is possible to effectively and accurately estimate inertia from ambient frequency and active power signals under normal operational fluctuations, rather than completely relying on large, infrequent disturbances. This allows for a continuous and real-time inertia monitoring.
- The considered ARMAX based estimation approach is able to provide relatively accurate inertia estimates even during transients produced by disturbances such as generator trips, load step changes, three-phase faults, and line disconnections.
- System identification techniques can be effectively applied to derive a transfer function that describes a certain active power-frequency relationship, from which an equivalent inertia constant can be extracted.
- The time varying values of virtual inertia contributions from CIG with VSM control can also be tracked continuously, which is crucial as inertia levels are becoming increasingly variable due to the high penetration of inverter-based resources.
- The efficacy of the implemented methods was successfully demonstrated on different sample test grids. By assessing the performance of the inertia estimation algorithms in real time, the research validates measurement-based alternatives that moves beyond offline studies, do not rely on disturbance events or require detailed mathematical models. This offers valuable insights on the practical aspects and potential of the considered approaches for actual real-world applications.

After completion of the project, the following main steps are envisioned:

- PMUs should include further functionalities to further exploit their measurements. Most importantly, the inclusion of an online trustworthiness metric (e.g., the nRMSE) would be beneficial both on a single-node and system-wise perspective. On the single-node perspective, it would allow for flagging measurements with higher measurement uncertainty. On a system-wise perspective, it would allow for associating different weights to measurements coming from nodes with higher noise and/or distortion.
- For inertia estimation application, one crucial step is represented by the identification of the signal portion affected by the power imbalance. Most methods require further post-processing of the PMU measurements whereas the PMU itself could indicate the instant where the disturbance has begun and the instant when the system has got back to quasi normal operation. This would expedite the online estimation of the inertia parameter. In order to obtain such result, it is important to develop clustering algorithms capable of splitting the PMU measurement results based not only on their geographical location but also on the type of waveforms they are observing.
- Large-scale power grids are vast and geographically dispersed, and the system inertia is distributed across the whole electrical grid. Therefore, the “effective” inertia is characterized by a decentralized nature that makes it vary locally in different areas. Then, decentralized inertia approximation strategies that can handle the dynamic and non-uniform inertia of specific power system regions, and enable a kind of online distributed multi-area inertia estimation, need to be further investigated.
- While PMUs provide high-resolution synchronized data, essential for real-time inertia estimation, their deployment is not abundant across very large grids. Therefore, the strategic location of PMUs

is critical to achieve enough observability with a minimum number of PMUs. Since this will directly impact the accuracy, cost-effectiveness, and real-time viability of the estimation process, further research is required to address the optimal location of PMUs.

- Furthermore, the quality, synchronization, and reliability of data from various sources across a vast area pose additional integration and processing challenges. Therefore, more investigation is needed in terms of related measurement errors, filtering effects, bad data, latency issues, communication failures, etc.

4 International cooperation

4.1 Strathclyde University, Glasgow, UK

The collaboration between the University of Strathclyde and the Swiss Federal Institute of Metrology (METAS), fostered within the framework of the ERI Grid 2.0 consortium, was not merely beneficial; it was essential for achieving the project's ambitious goals of creating a trustworthy and verifiable measurement and analysis chain for Transmission System Operators (TSOs). On one hand, the University of Strathclyde provides unparalleled expertise in the simulation and emulation of complex and realistic power system scenarios. Strathclyde's high-fidelity real-time digital simulators (RTDS) create a controlled, deterministic environment where these challenging events can be generated with precision and repeatability. In essence, Strathclyde creates the authentic grid conditions that new technologies must prove they can handle, moving validation far beyond simplistic, steady-state laboratory tests.

On the other hand, METAS brings the indispensable expertise of a National Metrology Institute, ensuring that the measurements are not just observed but are also rigorously understood and quantified. While a power system engineer can confirm that a PMU's output looks correct, a metrologist asks a more fundamental question: "How correct is it, and with what level of confidence?" METAS's contribution is centered on the characterization of measurement uncertainties, particularly under the very dynamic conditions created by Strathclyde. Traditional instrument calibration often relies on stable, sinusoidal signals at a nominal frequency. However, the true performance of a PMU is revealed during fast-changing events. METAS provides the advanced methodologies to model and quantify the un-certainties inherent in the measurement of dynamic phasors, frequency, and ROCOF, ensuring traceability to national standards. This metrological rigor is the bedrock of trust; it transforms an engineering validation into a scientifically robust verification, providing TSOs with the quantifiable confidence needed to integrate these new data streams into critical operational decisions.

This symbiotic partnership bridges the critical gap between system simulation and measurement science. Strathclyde provides the "what to measure"—the complex, realistic events—while METAS provides the framework for understanding "how well we are measuring it." Without Strathclyde's dynamic scenarios, METAS would be limited to characterizing instruments under conditions that do not reflect their intended use. Conversely, without METAS's metrological analysis, the validation results from the HIL tests would lack the quantifiable proof of accuracy and reliability required for standardization and industry-wide adoption. The ERI Grid 2.0 consortium was the crucial enabler, creating the platform for these two centres of excellence to fuse their expertise. This collaboration has therefore not only validated a specific set of PMU-based metrics but has also established a benchmark methodology for the holistic testing of smart grid measurement systems, ultimately accelerating the transition to a more observable and secure energy future.

4.2 University of Trento, Trento, Italy

The strategic collaboration between the University of Trento and the Swiss Federal Institute of Metrology (METAS) combined cutting-edge theory with metrological science. The University of Trento served as the theoretical engine of this collaboration, bringing its profound expertise in advanced signal processing, statistical estimation, and distributed systems theory. Their primary role was to develop the foundational algorithms for intelligent measurement aggregation. This involved moving beyond simple averaging to design sophisticated data fusion techniques that could optimally combine synchrophasor data streams from multiple, geographically dispersed nodes. The theoretical framework developed by Trento accounts for the spatial-temporal correlations between measurements, effectively creating a weighted, dynamic estimation of the "center of inertia" frequency for a region.

However, a theoretically elegant algorithm is of little practical use to a Transmission System Operator (TSO) without a quantifiable guarantee of its performance and reliability. This is where the indispensable contribution of METAS came to the forefront. As a National Metrology Institute, METAS anchored the theoretical work in the rigorous principles of measurement science. Their critical task was to develop a formal procedure for the aggregation process, ensuring that the final, consolidated frequency and ROCOF values were not only more accurate but also possessed a well-defined and traceable measurement uncertainty. METAS's expertise in uncertainty propagation was crucial for determining how the individual uncertainties of each PMU in the network combine and translate into a final uncertainty for the aggregated value. They established the methodologies for validating the performance of Trento's algorithms, defining the protocols to assess their accuracy, bias, and robustness under various simulated grid conditions.

This partnership created a powerful and essential feedback loop. The University of Trento's algorithms provided the innovative method for aggregation, while METAS provided the framework to prove their worth, transforming a promising academic concept into a trustworthy, metrologically sound procedure. The result of this collaboration is a significant leap forward: a validated, rigorous methodology for producing a single, high-confidence regional frequency measurement.

5 Publications and other communications

[A] M. Ramirez-Gonzalez, F.R. Segundo, P. Korba, Data-driven algorithms for real-time inertia estimation and prediction of frequency stability metrics, Book Chapter in "Advanced Testing of Complex Cyber-Physical Systems using OPAL-RT Framework." *In preparation.*

[B] M. Ramirez-Gonzalez, F.R. Segundo, P. Korba, Continuous Real-time Inertia Estimation in Power Systems Using ARMAX, ARX, and OE Models. *Submitted to Energy Reports Journal.*

[C] F. R. Segundo Sevilla, P. Korba, M. Ramirez-Gonzalez, G. Frigo, *et al.*, "Data Analytics in Low-Inertia Power Systems," *Submitted to the International Journal of Electrical Power and Energy Systems*.

[D] G. Frigo, P. Attilio Pegoraro and S. Toscani, "PMU Algorithms Based on Adaptive Taylor–Fourier Models: A Three-Phase Compressive Sensing Method for Spectral Support Recovery," in IEEE Transactions on Instrumentation and Measurement, vol. 74, pp. 1-14, 2025, Art no. 9003014, https://doi.org/10.1109/TIM.2025.3552878

[E] Grasso Toro, Federico, and Guglielmo Frigo. 2025. "Synthetic PMU Data Generator for Smart Grids Analytics" Metrology 5, no. 1: 12. https://doi.org/10.3390/metrology5010012

[F] P. Castello, G. Frigo, D. Sitzia and S. Sulis, "Characterization of Matrix Profile Technique for Enhanced Detection of Events in Sampled Values Data Streams," in IEEE Transactions on Instrumentation and Measurement, vol. 74, pp. 1-10, 2025, Art no. 9005110, doi: 10.1109/TIM.2025.3568960

[G] G. Frigo, D. Macii and D. Petri, "Dynamic Estimation and Fusion of Frequency and ROCOF Data via Local Gossiping," 2025 IEEE 15th International Workshop on Applied Measurements for Power Systems (AMPS), Bucharest, Romania, 2025, pp. 1-6, doi: 10.1109/AMPS66841.2025.11219911

[H] G. Frigo, Z. Feng, Y. Seferi and G. Burt, "Evaluation of Delay Time in PMU Prototypes for Hardware-in-the-Loop Testing," 2025 IEEE 15th International Workshop on Applied Measurements for Power Systems (AMPS), Bucharest, Romania, 2025, pp. 1-6, doi: 10.1109/AMPS66841.2025.11219909

[I] G. Frigo, G. Gallus, P. A. Pegoraro and S. Toscani, "Combining Steady-State Accuracy and Responsiveness of PMU Estimates: An Approach Based on Left and Right Taylor–Fourier Expansions," in IEEE Transactions on Instrumentation and Measurement, vol. 73, pp. 1-13, 2024, Art no. 9002713, doi: 10.1109/TIM.2024.3384553

[J] G. Frigo, P. Castello, G. Gallus, P. A. Pegoraro and S. Toscani, "Internal Time Reference Enhancement via White Rabbit Synchronization: A Power System Measurement Perspective," 2024 International Conference on Smart Grid Synchronized Measurements and Analytics (SGSMA), Washington, DC, USA, 2024, pp. 1-6, doi: 10.1109/SGSMA58694.2024.10571544

[K] M. Agustoni and G. Frigo, "Characterization of Analog Front-End in PMU Design for Inertia Monitoring," 2024 IEEE International Instrumentation and Measurement Technology Conference (I2MTC), Glasgow, United Kingdom, 2024, pp. 1-6, doi: 10.1109/I2MTC60896.2024.10560540

[L] A. Morato, G. Frigo and F. Tramarin, "5G-Enabled PMU-Based Distributed Measurement Systems: Network Infrastructure Optimization and Scalability Analysis," in IEEE Transactions on Instrumentation and Measurement, vol. 73, pp. 1-12, 2024, Art no. 5504212, doi: 10.1109/TIM.2024.3457959

[M] G. Frigo et al., "Validating Inertia Assessment Metrics in Distribution Systems with High RES Penetration," 2024 IEEE 14th International Workshop on Applied Measurements for Power Systems (AMPS), Caserta, Italy, Sept. 2024, pp. 1-5, doi: 10.1109/AMPS62611.2024.10706692.

[N] G. Frigo, D. Macii and D. Petri, "An Uncertainty-based Criterion for Aggregation of Consistent ROCOF Measurements," 2024 International Conference on Smart Grid Synchronized Measurements and Analytics (SGSMA), Washington, DC, USA, May 2024, pp. 1-6, doi: 10.1109/SGSMA58694.2024.10571405.

[O] F. Costa, G. Frigo, D. Husmann, A. Jallageas and J. Morel, "Comparison of Time Synchronization Sources for PMU Calibration Infrastructures," 2023 IEEE International Symposium on Precision Clock Synchronization for Measurement, Control, and Communication (ISPCS), London, United Kingdom, 2023, pp. 1-6, doi: 10.1109/ISPCS59528.2023.10297016

[P] G. Frigo, G. Gallus, P. A. Pegoraro and S. Toscani, "Improving Step Performance of PMU Algorithms: Left and Right Taylor-Fourier Expansions," 2023 IEEE 13th International Workshop on Applied Measurements for Power Systems (AMPS), Bern, Switzerland, 2023, pp. 01-06, doi: 10.1109/AMPS59207.2023.10297128

[Q] G. Frigo and F. Grasso-Toro, "Feasibility Analysis of Online Uncertainty Metrics for PMU-Based State Estimation," October 2023, Applied Sciences 13(21):11670.

[R] G. Frigo, F. Costa and F. Grasso-Toro, "Phasor measurement unit based reliability index for renewable-based power systems," Sept. 2023, ACTA IMEKO 12(3):1-7.

[S] F. Costa, L. Peretto and G. Frigo, "PMU-Based Estimation of Inertia Variation: Proposed Metric and Feasibility Analysis," May 2023, IEEE International Instrumentation and Measurement Technology Conference (I2MTC), Kuala-Lumpur, Malaysia.

[T] F. Costa and G. Frigo, "Interoperability Issues in PQ and PMU Measurements for Reduced Inertia Power Systems," May 2023, IEEE International Instrumentation and Measurement Technology Conference (I2MTC), Kuala-Lumpur, Malaysia.

[U] F. Costa and G. Frigo, "Local Aggregation of PMU Measurements in a Low-Inertia Distribution Power System," April 2023, 4th International Conference on Smart Grid Metrology (SMAGRIMET), Dubrovnik, Croatia.

[V] G. Frigo, F. Costa and F. Grasso-Toro, “PMU-based metrics for Power Quality Assessment in Distributed Sensor Networks,” September 2022, 25th IMEKO TC4 International Symposium, Brescia, Italy.

[W] G. Frigo and F. Grasso-Toro, “Metrological Significance and Reliability of On-Line Performance Metrics in PMU-based WLS State Estimation,” May 2022, International Conference on Smart Grid Synchronized Measurements and Analytics (SGSMA), Split, Croatia.

6 References

[1] F.R. Segundo Sevilla, Y. Liu, E. Barocio, P. Korba et al., 2022, “State-of-the-art of data collection, analytics, and future needs of transmission utilities worldwide to account for the continuous growth of sensing data”, International Journal of Electrical Power and Energy Systems, Vol. 137, pp. 107772, ISNN 0142-0615.

[2] Swiss Federal Office of Energy, 2018, "Energy strategy 2050 once the new energy act is in force," Online: Energy Strategy 2050 (admin.ch).

[3] Christoph Rüeger, Jean Dobrowolski, Petr Korba, Felix Rafael Segundo Sevilla, 2021. “Analysis of grid events influenced by different levels of renewable integration on extra-large power systems”, Advances in Science, Technology and Engineering Systems Journal, Vol. 6, no. 5, pp. 43-52, 2021.

[4| M. Paolone, T. Gaunt, X. Guillaud, M. Liserre et al., 2020 "Fundamentals of power systems modelling in the presence of converter-interfaced generation," Electric Power Systems Research, Vol. 189, pp. 106811, ISSN 0378-7796. DOI: https://doi.org/10.1016/j.epsr.2020.106811

[5] Novel Analysis and Control Solutions for Dynamic security issues in the future ENTSO-E network with high converter-based generation," Online: ACSICON Novel Analysis and Control Solutions for Dynamic Security Issues in the future - Participants (admin.ch).

[6] E. Farantos, P. Dattaray and M. Patel, 2021, "PMU Based Inertia Estimation and Monitoring," NASPI Work Group Meeting, Online: PowerPoint Presentation (naspi.org).

[7] G. Frigo, A. Derviškadić, Y. Zuo and M. Paolone, "PMU-Based ROCOF Measurements: Uncertainty Limits and Metrological Significance in Power System Applications," in IEEE Transactions on Instrumentation and Measurement, vol. 68, no. 10, pp. 3810-3822, Oct. 2019.

[8] A. Derviškadić, G. Frigo and M. Paolone, "Beyond Phasors: Modeling of Power System Signals Using the Hilbert Transform," in IEEE Transactions on Power Systems, vol. 35, no. 4, pp. 2971-2980, July 2020.

[9] IEC/IEEE 60255-118-1:2018, "Measuring relays and protection equipment - Part 118-1: Synchro-phasor for power systems – Measurements"

[10] J. Machowski, Z. Lubosny, J. W. Bialek, J. R. Bumby, Power System Dynamics Stability and Control. NJ: Wiley, 2020

[11] A. Dixon, Modern Aspects of Power System Frequency Stability and Control. UK: Academic Press, 2019.

[12] A. Monti, F. Milano, E. Bompard, X. Guillaud, Converter-Based Dynamics and Control of Modern Power Systems. UK: Academic Press, 2021.

[13] P. Denholm, T. Mai, R. Wallace, B. Kroposki, M. O’Malley. “Inertia and the Power Grid: A Guide Without the Spin”, Tech. Rep. NREL/TP-6A20-73856, 2020.

[14] B. Tan, J. Zhao, M. Netto, V. Krishnan,V. Terzija, Y. Zhang, “Power system inertia estimation:

Review of methods and the impacts of converter-interfaced generations," International Journal of Electrical Power and Energy Systems, vol. 134 (4), 2021.

[15] K. Tuttelberg, J. Kilter, D. Wilson, K. Uhlen, "Estimation of Power System Inertia from Ambient Wide Area Measurements," IEEE Transactions on Power Systems, vol. 33 (6), pp. 7249-7257, 2018.

[16] V. Sagar, S. K. Jain, "System Identification-based Estimation of Power System Inertia Using PMU Data," 21st National Power Systems Conference, pp. 1-6, Dec. 2020.

[17] D. Giudice, S. Grillo, "Analysis of the Sensitivity of Extended Kalman Filter-Based Inertia Estimation Method to the Assumed Time of Disturbance," Energies, vol. 12, pp. 1-19, 2019.

[18] G. Rossetto, F. Pozzi, V. Ilea, A. Berizzi, E. Carlini, G. Giannuzzi, R. Zaottini, "Measurement-based inertia estimation method considering system reduction strategies and dynamic equivalents," IEEE Milan PowerTech, pp. 1-6, June 2019.

[19] M. Hayerikhiyavi, A. Dimitrovski, "A practical assessment of the power grid inertia constant using PMUs," 52nd North American Power Symposium, pp. 1-5, April 2021.

[20] Z. Lin, C. Hong, C. Guo, "Equivalent Inertia Estimation of Power System Based on Kinetic Energy Theorem," IEEE International Conference on Power Science and Technology, pp. 1-6, May 2023.

[21] E. Raju, H. Marzooghi, J. Yu, V. Terzija, "Development and Validation of Artificial Neural Network-Based Tools for Forecasting of Power System Inertia With Wind Farms Penetration," IEEE Systems Journal, vol. 14 (4), pp. 4978-4989, 2020.

[22] M.Tuo, X. Li, "Machine Learning Assisted Inertia Estimation Using Ambient Measurements," IEEE Trans. On Industry Applications, vol. 59 (4), pp. 4893-4903, 2023.

[23] L. Ljung, System Identification: Theory for the User. NJ: Prentice Hall, 1999.

[24] D. I. Wilson, Advanced Control using MATLAB. New Zealand: Auckland University of Technology, 2016.

[25] S. Kellermüller, A. Obushevs, M. Ramirez-Gonzalez, P. Korba, "Digital Twin Development of a Dynamic Hardware Emulator," Energies, vol. 15, no. 13, 2022.

[26] DIgSILENT GmbH, DIgSILENT PowerFactory, Version 2025 SP2.

[27] M. Ramirez-Gonzalez, F. R. Segundo Sevilla, P. Korba, "Power System Inertia Estimation Using a Residual Neural Network Based Approach," 4th Global Power, Energy and Communication Conference- GPECOM2022, Cappadocia, Turkey, June 14-17, 2022.

[28] MATLAB/Simulink, Version 23.2.0 (R2023b). The MathWorks, Inc.

[29] ePHASORSIM, Large-Scale Electromechanical Power System Real-Time Simulation. [Online] https://www.opal-rt.com/systems-ephasorsim/

[30] Typhoon HIL, Documentation: Grid-connected inverter with virtual synchronous machine. V2024.3, Typhoon HIL, Inc.